Biochemistry and Chemical Biology

Induction of Hepatitis B Core Protein Aggregation Targeting an Unconventional Binding Site

Vladimir Khayenko, Cihan Makbul, Clemens Schulte, Naomi Hemmelmann, Sonja Kachler, Bettina Böttcher, Hans M Maric

Rudolf Virchow Center, Center for Integrative and Translational Bioimaging; University of Würzburg, Würzburg Germany • Biocenter, University of Würzburg, Würzburg, Germany

Reviewed Preprint
v2 • January 23, 2025
Revised by authors

Reviewed Preprint
v1 • July 5, 2024

eLife Assessment

This **valuable** work presents an interesting strategy to interfere with the HBV infectious cycle as it identifies two previously unexplored HBc-Ag binding pockets. The experimental data is **compelling** and opens the door to generating and testing novel anti-HBV therapies.

https://doi.org/10.7554/eLife.98827.2.sa3

Abstract

The hepatitis B virus (HBV) infection is a major global health problem, with chronic infection leading to liver complications and high death toll. Current treatments, such as nucleos(t)ide analogs and interferon-α, effectively suppress viral replication but rarely cure the infection. To address this, new antivirals targeting different components of the HBV molecular machinery are being developed. Here we investigated the hepatitis B core protein (HBc) that forms the viral capsids and plays a vital role in the HBV life cycle. We explored two distinct binding pockets on the HBV capsid: the central hydrophobic pocket of HBc-dimers and the pocket at the tips of capsid spikes. We synthesized a geranyl dimer that binds to the central pocket with micromolar affinity, and dimeric peptides that bind the spike-tip pocket with sub-micromolar affinity. Cryo-electron microscopy further confirmed the binding of peptide dimers to the capsid spike tips and their capsid-aggregating properties. Finally, we show that the peptide dimers induce HBc aggregation in vitro and in living cells. Our findings highlight two tractable sites within the HBV capsid and provide an alternative strategy to affect HBV capsids.

Introduction

The hepatitis B virus (HBV) infects the liver and can cause acute and chronic hepatitis. In childhood and infancy, the virus is particularly dangerous, as the recovery rate among children is approximately 50%, while among infants infected through perinatal transmission, only 10% will

naturally recover, the remainder will develop chronic infection.[1,2] On the global scale the most effective approach to address hepatitis B is through preventive treatment with vaccinations. However, the goals of achieving sufficient vaccination coverage and timely immunization have yet to be met.[1,3] Furthermore, vaccinations are ineffective for individuals who are already infected.[4] With about 300 million chronic carriers and over 800,000 hepatitis-related yearly deaths, chronic hepatitis B is a global health problem[2,5] that requires a solution. Currently, there are two approved classes of medications for the treatment of chronic hepatitis B: nucleos(t)ide analogs (NAs) and interferon-α and its derivatives (IFN-α).[6,7] NAs compete for binding with the natural nucleotide substrates, inhibiting the viral protein P in charge of the reverse transcription of the viral pre-genomic RNA (pgRNA) into HBV DNA.[8] IFN-α serves as both an immunomodulator and immunostimulant, activating genes with diverse antiviral functions to target various steps of viral replication. Additionally, it indirectly suppresses HBV infection by modifying cell-mediated immunity.[9]

Present treatments effectively suppress HBV replication, reduce liver inflammation, fibrosis, and the risk of cirrhosis and hepatocellular carcinoma (HCC), but IFN-α treatment is associated with significant adverse effects and NAs typically require long-term oral administration, often lifelong, as treatment discontinuation often results in viral rebound and disease recurrence in many patients. While current therapies manage the disease, a clinical cure is seldom achieved, and the risk of HCC, although reduced, remains.[7] Consequently, various classes of direct-acting antivirals and immunomodulatory therapies are currently under development, aiming to achieve a functional cure following a finite treatment duration.[10]

New HBV antivirals capitalize on the enhanced understanding of the viral life cycle and can be categorized into several classes (**Table 1**): Entry inhibitors that disrupt HBV entry into hepatocytes by blocking the binding to the sodium/taurocholate co-transporting polypeptide (NTCP) receptor.[11] HBsAg inhibitors based on nucleic acid polymers that interfere with the production of HBV surface antigens, and viral gene repressors based on nucleases. Translation inhibitors based on small interfering RNAs or antisense oligonucleotides that silence HBV RNA, thereby decreasing the viral antigen production. Finally, the capsid assembly modulators (CAMs) target the hepatitis B core protein (HBc) that participates in multiple essential steps of the HBV life cycle.[7]

Among the direct acting antivirals that are in preclinical or clinical studies, a third are CAMs.[6] Capsids are attractive targets due to the absence of human homologues for HBc and their involvement in crucial stages of the HBV life cycle, including nuclear entry, encapsulation of the pgRNA and polymerase, optional nuclear recycling to replenish the covalently closed circular DNA (cccDNA) pool, and eventual coating and secretion from infected cells.[7,22]

The capsid is composed of 120 units of HBc dimers, assembling into a T = 4 icosahedron. Within this structure, 60 asymmetric units are formed by 4 HBc monomers each, designated as A, B, C, and D, or AB dimers and CD dimers.[25] The ultrastructure formed by the HBc dimer reveals several binding pockets that can be exploited as potential targets for modulating protein activity (**Figure 1**).

CAMs target the hydrophobic pocket at the HBc dimer-dimer interface, upon binding they strengthen the association energy between HBc-dimer subunits, thereby promoting capsid assembly, rather than inhibiting it.[26,27] As a result, abnormal or empty capsids may form, sometimes accompanied by the aggregation of core proteins, consequently inhibiting HBV DNA replication. Additionally, CAMs can disrupt the disassembly of incoming virions and the intracellular recycling of capsids, thereby impeding the establishment and replenishment of cccDNA.[7,22,28,29]

Table 1.

Direct-acting HBV antivirals

Class	Mechanism of action	Examples	Development stage[6]	Molecule type
Entry Inhibitors	NTCP (sodium/taurocholate co-transporting polypeptide) receptor[12] inhibition.	Bulevirtide[13]	Phase III	Lipopeptide
		A2342[14]	Preclinical	Small molecule
HBsAg inhibitor	Inhibition of the host HSP40 chaperone DNAJB12, that mediates spherical HBV assembly. Reduces the HBsAg in the circulation and lowers intracellular HBsAg.[15]	REP 2139[16]	Phase II	Nucleic acid polymer
Translation inhibitors	Antisense oligonucleotide (ASO) or small interfering RNAs (siRNA)[17] that target HBV messenger RNAs and act to decrease levels of viral proteins.	Bepirovirsen [18]	Phase III	ASO
		VIR-2218[19]	Phase II	siRNA
Viral gene repressors	Specific cleavage mediation of viral covalently closed circular DNA (cccDNA) via nucleases.[20]	PBGENE-HBV[21]	Preclinical	Endonuclease I-CreI
		EBT107[20]	Preclinical	CRISPR-Cas9
Capsid assembly modulators	Target the hydrophobic pocket located at the dimer-dimer interface near the C termini of HBc subunits and induce misassembly of the core protein, thereby impeding the formation of infectious progeny virions. [20,22,23]	Canocapavir[23]	Phase II	Small molecule
		EDP-514[24]	Phase I	Small molecule

Figure 1.

HBc binding pockets and mode of action of dimeric binders.

A) Left: Close-up view of the three addressable effector sites within HBc-dimers (shown as cartoon model with transparent surface in grey) together with representative ligands shown as stick models: SLLGRM peptide (marine blue, PDB: 7PZN); Geraniol, resolved here (Cyan); heteroaryldihydropyrimidine (HAP ((2S)-1-[[(4R)-4-(2-chloranyl-4-fluoranyl-phenyl)-5-methoxycarbonyl-2-(1,3-thiazol-2-yl)-1,4-dihydropyrimidin-6-yl]methyl]-4,4-bis(fluoranyl)-pyrrolidine-2-carboxylic acid), green, PDB: 5WRE). HAP is a representative example of a canonical CAM, that targets a hydrophobic pocket mediating HBc-dimer multimerization, an essential step in capsid assembly. A blue arrow indicates how dimeric peptide-based ligands may induce aggregation. Right: The general architecture of an HBc-dimer is depicted as a cartoon with transparent surface model in grey and the three ligands that target distinct binding pockets are in color. The binding sites of two HBc dimers can be linked by dimeric ligands, here exemplified with the peptide ligand. B) Hypothetical mode of action of HBc aggregation triggered by cross linking the spikes of individual HBc dimers, HBc multimers or the whole capsid.

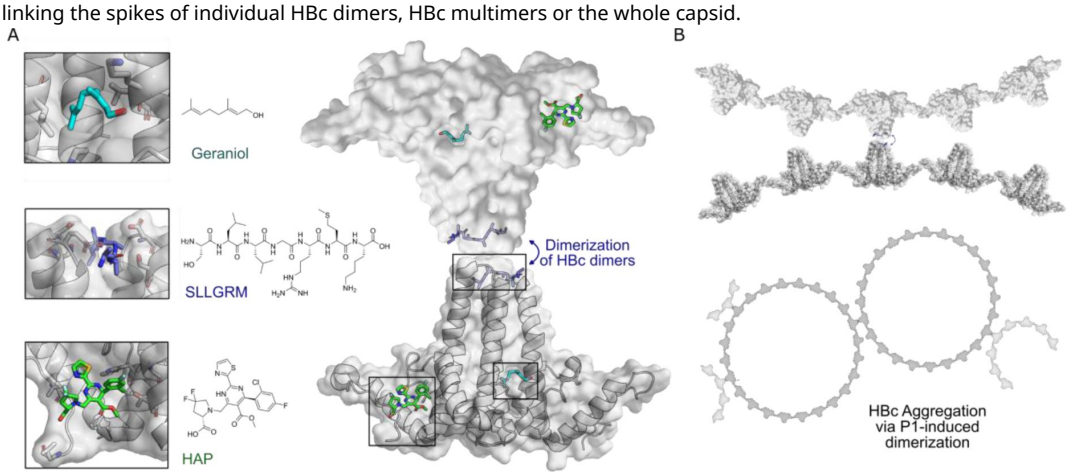

Recently, a new potentially druggable site was discovered in the HBc dimer – a hydrophobic pocket formed at the base of the spike. This site was targeted by the detergent Triton X-100 (TX100), ultimately causing conformational alterations in the capsid structure.[30,31] In addition to the spike base hydrophobic pocket, there is another less-explored interacting domain located on the spike tip of the HBc dimer. Previous studies have shown that peptides targeting the cleft on the spike tip reduced viral replication in a cell model, likely by interfering with viral assembly through modulation of the HBc interaction with the surface antigen.[32] These two effector sites could serve as a foundation for the development of new types of HBc modulators and provide alternatives ways for controlling HBV infections.

In this study, we characterize and explore these alternative HBc binding pockets at the inner-dimer interface in the center and at the tips of capsid spikes[30,31,33], and unveil the HBc aggregating properties of a spike-binding dimeric peptide.

Results

HBV capsid assembly modulation via the binding pockets on the HBc multimer ultrastructure represents a promising pharmacological strategy but until now only one site located on the HBc dimer-dimer interface was explored (**Figure 1A**).[22,23] We designed and synthesized bivalent binders specifically targeting two distinct regions of the HBV core protein (HBc)—the hydrophobic pocket at the dimer interface and the tips of the capsid spikes (**Figure 1**). These binders, designed to engage both sites with avidity enhanced affinity, were evaluated for their binding affinity and their effects on HBV capsids in both in vitro assays and living cell models.

Geranyl dimer targets the central hydrophobic pocket of HBc-dimers with micromolar affinity

Hydrophobic post-translational modifications, such as myristylation of the Large Hepatitis B Virus Surface Protein (L-HBs), are essential for HBV infectivity and play a role in mediating viral assembly.[34] Additionally, farnesylation, another hydrophobic post-translational modification, is involved in the envelopment of hepatitis D virus (HDV)[35], which relies on the presence of HBV and its protein machinery for propagation. Recently, TX100, a nonionic surfactant sharing a similar hydrocarbon binding motif as the natural HBV post-translational modifications, was identified as a ligand of a distinct hydrophobic pocket in the center of HBc-$_{dimers}$.[30,31,36,37]

Several of the pocket forming amino acids, such as K96 and 129-PPAY-132,[38] and the natural occurring point mutations HBcP5T, L60V, F97L and P130T[37,39–42] are involved in secretion of enveloped virions from the cell. These findings lead to the infectious HBV particles signal hypothesis where this hydrophobic pocket is involved in the regulation of the envelopment of nucleocapsids and thus could be an alternative druggable pocket to block virus envelopment.[36]

We reasoned that compounds mimicking the natural HBV/HDV compounds and sharing a hydrophobic motif similar to that of TX100 can prove to be potent binders of this key hydrophobic pocket. Therefore, we set out to test n-Decyl-beta-D-maltopyranoside (DM) (1), geraniol (2) and its synthesized dimer (3), as the mimetics of myristic acid and farnesyl, respectively.

The isothermal calorimetric titration (ITC) of HBc capsids with DM (1) resolved micromolar affinity (K_D = 133 +/− 38 μM) to all four hydrophobic pockets of HBc capsids' asymmetric unit (N=1.05 +/− 0.1) (**Figure 2B** and **Supplementary Figure 7C**). ITC of geraniol with HBc showed a slightly enhanced micromolar affinity (K_D=94 +/− 8 μM) (**Figure 2A,B**, **supplementary tables 1**, **2** and **Supplementary Figure 7A,B**) and a stoichiometry of N=1.01 +/− 0.04, implying that all four hydrophobic pockets of the asymmetric unit are occupied simultaneously. To confirm

geraniol's binding to the capsids and to resolve the molecular details of this interaction we conducted cryo-EM of a mixture of HBc with excess of geraniol followed by single particle analysis. This experiment resolved an additional density for geraniol in all four hydrophobic pockets within the asymmetric unit of HBc capsids (**Figure 2D**, **Supplementary Figure 8**), confirming the thermodynamic binding data and further defining the underlying molecular interactions of the involved HBV residues P5, L60, K96 and F97.

Encouraged by structural confirmation of geraniol binding to the central hydrophobic pocket, we designed and synthesized a dimeric version of geraniol potentially capable of simultaneous binding to the HBc dimer. We connected the two geranyl moieties with a polyethylene glycol (PEG) linker that could bridge the distance of 38 Å between the two opposing hydrophobic pockets (see **Supplementary Figure 1** for the design rationale). After synthesis, purification and mass spectrometric validation (**Appendix 1**) we determined the HBc capsid binding parameters of the geranyl dimer via ITC. The analysis suggested that the dimer engages with both HBc binding sites simultaneously, resulting, however, only in a moderately enhanced micromolar affinity of 63 +/− 8 µM (**Figure 2B**).

Targeting the pocket of capsid spike tips with sub-micromolar affinity peptide dimers

Although geraniol and geranyl dimer displayed improved affinity to HBc and allowed structural insights on a binding pocket located at the center of HBc dimers, micromolar affinity is sub-optimal for a functional compound. Therefore, we proceeded to explore another binding site located on the capsid spike tips formed by HBc dimers (**Figure 1**).[32]

Earlier studies have shown that phage display-derived peptides were binding to the spike tips of recombinant HBc capsids. These peptides were also observed to disrupt the interaction between HBc and HBV's surface protein, L-HBs.[43] Recently we have shown that these peptides MHRSLLGRMKGA (P1), GSLLGRMKGA (P2) and the core binding motif SLLGRM bind to wild-type (wt) and mutant HBc variants (P5T, L60V and F97L) with intermediate micromolar K_Ds of 26, 68 and 130 µM, respectively.[33]

Here, we designed dimeric peptides with a PEG linker capable of bridging the distance of 50 Å between the capsid spikes, thus tailoring our binders for simultaneous binding of two HBc dimers (**Figure 1B**, **Supplementary Figure 1**). The three distinct dimeric peptides, the minimal SLLGRM dimer (4), the P2 dimer (P2d) (5), and two P1 dimers (P1d) (**6**) and P1dC (**7**), were synthesized, purified, and validated using mass spectrometry (**Appendix 1**). Subsequently, their binding to the HBV capsid was evaluated through ITC (**Figure 3A**, **Supplementary Table 2**, **Supplementary Figures 3**,**7**). With a K_D value of 4.9 +/− 0.7 µM, the SLLGRM-dimer (**4**) has the lowest affinity to HBc, followed by the P2-dimer (**5**) (K_D =1.9 +/− 0.4 µM). Finally, the P1-dimers (**6**) and (**7**) displayed sub-micromolar affinities of 312 nM and 420 nM. Thus, P1-, P2- and SLLGRM-dimers show 83-, 36- and 27-fold increased affinities compared to their monomeric counterparts.

The significant increase in affinity of the P1-dimer over the monomer, by almost two orders of magnitude, may not be solely attributed to binding to two sites simultaneously. Once the P1-dimer binds it can interact with up to four binding partners in its vicinity (**Supplementary Figure 5**).[44] This may enable detachment and immediate reattachment to a nearby binding partner, further enhancing the local concentration and the overall binding strength of the P1 dimer. Finally, our Cryo-EM experiments have confirmed that the peptide dimers occupy the binding site at the spike tip of HBc dimers. Among these, the dimerized P1 exhibited a higher occupation of the binding site, as illustrated for P1dC (7) in **Supplementary Figure 9**.

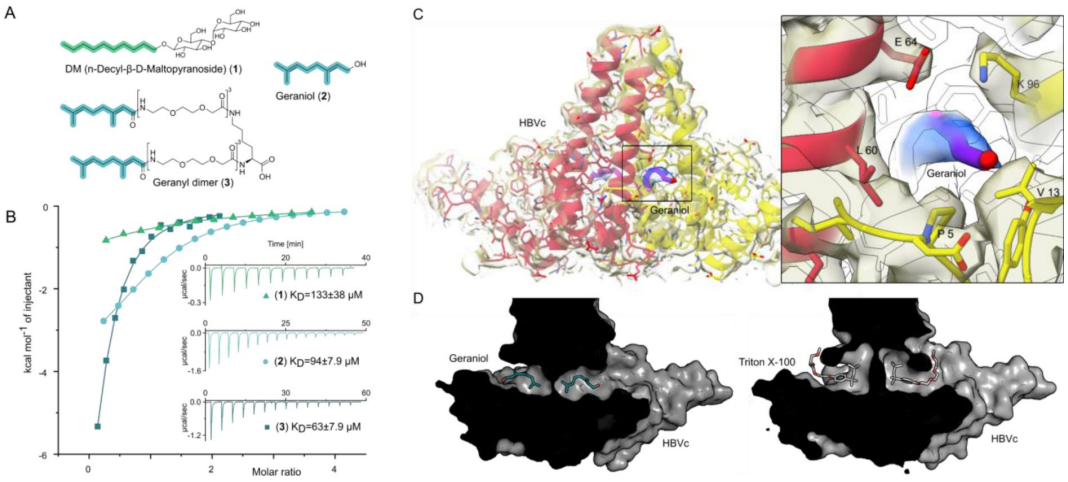

Figure 2.

The central hydrophobic pocket of HBc-dimer is targeted by hydrophobic molecules containing isoprene units.

A) Structures of different substances used for the ITC and cryo-EM experiments. N-Decyl-beta-D-maltopyranoside (DM) (1) and geraniol (2). Using geranic acid we synthesized geranyl dimer (**3**), a dimeric binder forked by a lysine and having a linker of six dioxaoctanoic units. B) Representative ITC heat signatures of DM (1), geraniol (2) and the geranyl dimer (**3**) with HBc capsids. Heat release is detected upon titration of the ligands to the HBc solution, indicating stoichiometric binding interaction. 4 mM geraniol (2) was titrated into a solution of 210 µM HBc. A solution of 2 mM geranyl dimer (3) was titrated into a solution 200 µM HBc. 1.6-2 mM solutions of DM (1) were titrated into solutions with 90, 100 and 150 µM HBc, respectively. The control experiments where geraniol, geranyl dimer and DM were titrated into buffer are shown in **Supplementary Figure 7**. Integrated heat signatures in kcal·mol^{-1} plotted against the molar ratio of titrants to HBc. Binding isotherms (solid lines) were determined using a curve fitting procedure based on a one-site model. Among the ligands, the geranyl dimer has the strongest affinity to HBc, expectedly surpassing the monovalent geraniol by 2-fold. C) Structure of the geraniol (magenta) within the HBc binding site (yellow and red) together with close-up view of the binding site with the EM-densities. Geraniol and residues (P5, L60, K96, E64 and V13) involved in HBV's envelopment with natural phenotypes are depicted in stick representation. The EM density of geraniol is shown in the zoom-out in blue. D) Side-by-side comparison of the overlapping HBc geraniol and TX100[31] binding sites suggests conformational flexibility and the ability of the hydrophobic pocket to accommodate larger hydrophobic molecules.

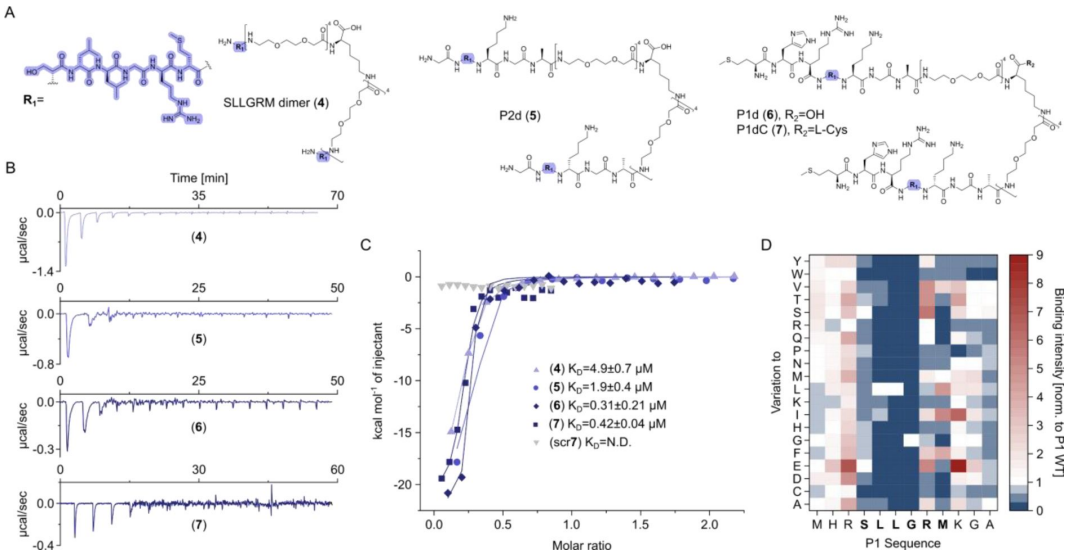

Figure 3.

Dimeric peptide spike binders display strong low micromolar and sub-micromolar affinity.

A) Chemical structures of the dimeric peptides, all contain the core binding sequence -SLLGRM and share the same PEG linker and a lysine as the branching element of the dimer. B) Exemplary ITC thermograms showing the titration heat signature of HBc with dimers. A solution of 1500 µM (**4**) was titrated into a solution 150 µM HBc. A solution of 125 µM (**5**) was titrated into a solution 25 µM HBc. A solution of 200 µM (**6**) was titrated into a solution 25 µM HBc. A solution of 100 µM (**7**) was titrated into a solution 25 µM HBc. C) The peptide dimers display low micromolar to sub-micromolar affinity to HBc, the affinity increases with the elongation of the binding sequence. D) Sequence requirements of the HBc Spike binding site. Full positional scan of the P1 peptide sequence in microarray format, in which each residue was varied to each other proteogenic amino acid. Note that a drop in binding intensity upon variation of the core motif SLLGRM (highlighted in bold) substantiates its critical involvement in HBc binding. Refer to **supplementary table 3** for the corresponding absolute greyscale values. Affinity gains observed for exchanging positively charged for negatively charged amino acids may be assay-specific false-positives as highlighted previously.[33]

Notably, while performing the ITC titrations we have noticed fast fluctuations of the heat signature baseline across the tested ligands (**Figure 3**; **Supplementary Figure 3**), at least for the P1 dimer this phenomenon may be attributed to aggregation. To rule out any non-specific interactions caused by the PEG linker or handle for both the geranyl dimers as well as the P1/2 dimers, a scrambled dimeric peptide was used as a negative control. This scrambled peptide showed no detectable binding (**Figure 3C**), thereby confirming that the observed binding is specific to the designed peptide sequence and not influenced by the linker or other structural components.

To further substantiate and quantify a possible dimer-induced HBc aggregation we next performed a turbidity assay.[45] We found that P1 dimer induces turbidity of a HBc solution already at 1:10 equivalents of HBc, whereas the P2 dimer was slightly less potent and the SLLGRM dimer did not induce turbidity at the same conditions and further required significantly higher concentrations ratio relative to HBc (**Supplementary Figure 2**). To shed light on the seemingly sequence-specific aggregation properties of the different dimers we analyzed the binding of 240-point mutated P1 peptide variants in array format (**Figure 3D**, **Supplementary Table 3**). The analysis recapitulated our earlier resolved sequence requirement for HBc binding and substantiated that the minimal sequence SLLGRM is the major mediator of HBc binding. Importantly, it further indicates that the additional N-terminal residues in P1 sequence are neither conserved nor critically required for binding despite their importance in inducing HBc aggregation.

P1dC aggregates HBc in living HEK293 cells

The sub-micromolar affinity of the P1-dimer, along with its ability to induce capsid aggregation *in vitro*, prompted us to evaluate its effect on HBV core protein in living cells. To adapt the peptide for the intracellular delivery, we synthesized a C-terminally cysteinated version of P1-dimer, P1dC (7) (**Figure 3A**), and its scrambled counterpart scrP1dC scr(7) as well as a thiol-reactive polyarginine-based cell penetrating peptide (CPP), containing a cysteine, with a 5-thio-2-nitrobenzoic acid (TNB) modified thiol (**Figure 4A**, **Appendix 1**). At the core of this intracellular delivery method is the in-situ conjugation of the cargo molecule to a molar excess of a CPP via a disulfide bond, and the application of this reaction mix on living cells. The excess of the CPP over the active compound enable the reaction of CPP-thiols with the cellular surface, facilitating the penetration of the cargo-CPP conjugate. In turn, the disulfide bond between CPP and the cargo is reduced in the cytosol, separating the cargo from the CPP, allowing unhindered activity of the cargo molecule within the cell (**Figure 4B**).[46,47]

To verify that the P1dC performs similarly to P1-dimer we performed another ITC assay to determine the affinity of the compound to HBc. The ITC confirmed that P1dC has an affinity of 420 +/−38 nM, comparable to P1-dimer, while the scrambled peptide did not display binding to HBc (**Figure 3**, **Supplementary Figure 3**, **Supplementary Table 2**). Thereafter we transfected mammalian cells (HEK293) with a plasmid coding for HBc. The cells expressed the protein for two days and were then treated for 1 hour with the thiol-activated cell penetrating peptide and P1dC or the respective negative control peptide scrP1dC (**Figure 4B**). Afterwards the cells were immediately washed and fixed and HBc was visualized with anti-HBc antibody and a secondary DyLight650 conjugated antibody. Transfected but otherwise untreated cells showed a homogeneous distribution of recombinant HBc molecules in the nucleus and to a lesser extent in the cytoplasm (**Figure 4C**). Yet, upon administration of 10 µM of P1dC (7), we observed aggregates of HBc (in form of large bright spots) within the cells (**Figure 4C**, **Supplementary Figure 4**). At a concentration of 10 µM, the scrambled dimer scrP1dC did not induce aggregation and the distribution of HBc remained largely homogenous.

Our live cell experiments have corroborated our in vitro findings, providing us a visual proof of P1dC-mediated HBc aggregation in a living cell. Thus, the peptide dimer causes an aggregation that resembles the HAP induced aggregation of the core protein and, like CAMs, can be expected to

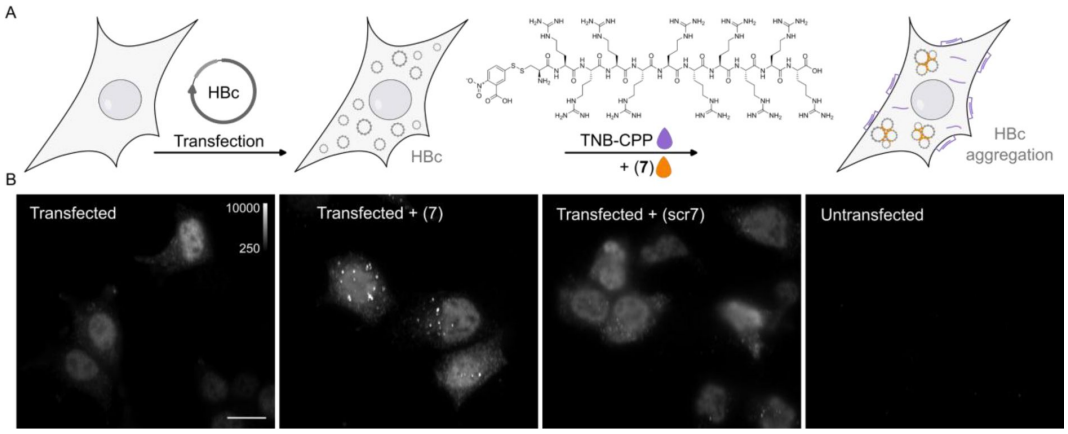

Figure 4.

P1dC aggregates HBc in living HEK293 cells.

A) A polyarginine cell-penetrating peptide containing a cysteine with a TNB-activated thiol (gray highlight, (**8**)). B) The live cell experiment flow. First, mammalian cells are transfected with HBc coding plasmid. Then, after the cells express the protein, a mix of (**8**) and (**7**) is applied. The excess CPP facilitates membrane permeation, allowing (**7**) to enter the cell after a brief incubation. Once inside, (**7**) is separated from the CPP and can interact with the capsids. C) After 1 hour incubation with (**7**) or scr(**7**) the cells were immediately washed, fixed and labelled with anti HBc mAb16988 and a secondary DyLight650 conjugated antibody. The cells were visualized on wide-field fluorescent microscope with identical conditions and are presented with the same grayscale range. Transfected and untreated cells display diffuse HBc distribution, with clear fluorescence at the nucleus. Transfected cells treated with (**7**) display bright aggregates, whereas transfected cells treated with scr(**7**) have similar diffuse labelling as the untreated cells. Non-transfected cells are non-fluorescent. Scale bar 20 μm.

have the potential to disrupt the HBV life cycle.

Cryo-EM confirms peptide-induced HBc aggregation

To affirm the capsid-aggregation property of our peptide dimers, we incubated solubilized purified capsid-like particles (CLPs, spherical capsid-like HBc multimers purified from E. coli) with an excess of SLLGRM-dimer or P1dC, applied them on carbon grids, and imaged them using cryo-EM. The effect of peptide dimers on CLPs was already seen on the microscale Cryo-EM images (**Supplementary Figure 9**), with P1dC inducing large protein aggregates with multimicron diameter. The less potent SLLGRM-dimer also induced visible aggregation, although with smaller aggregate size, while geraniol-treated samples showed minimal aggregation, and the smallest observed aggregate sizes. In the nanoscale we observed clumped CLPs (**Supplementary Figure 10A,B**) and resolved the binding of both peptide dimers to the spike tips (**Supplementary Figure 10C,D**, **Figure 5**). The densities corresponding to bound peptide-dimers in both EM-reconstructions have volumes which can accommodate a peptide chain of approximately 6 amino-acid residues (**Figure 5** and **Supplementary Figure 10C,D**).

The asymmetric unit of HBc capsids (T=4) is a tetramer consisting of an A/B- and C/D-dimer which have slightly different 3D-structures. Interestingly, the SLLGRM-dimer binds the A/B-dimer as well as the C/D-dimer, in contrast to the monomeric SLLGRM which binds only to the tip of the C/D-dimer[33],(**Figure 5**) in line with the multivalent binding and the higher affinity we measured with ITC. A possible mode of action of the peptide-dimer induced aggregation is shown in **Figure1B**.

The live cell experiments showed the formation of HBc aggregates upon incubation with P1dC. Yet, in live cells HBc may exist as a monomer, a dimer, a multimer or a whole capsid, therefore, the observed aggregates were not necessarily formed by whole capsids. The Cryo-EM experiment, however, provides confirmation that the peptide dimers have the capability to interact with complete CLPs, an important feature, that implies that the dimers have the potential to affect intact capsids upon cell infection.

Discussion

In this study, we focused on the HBV core protein, a protein essential for HBV proliferation and virulence. We explored the druggability of two alternative, non-HAP, binding pockets on the HBc ultrastructure and developed synthetic dimers that target these pockets with sub-micromolar affinity resulting in the aggregation of HBc.

DM and Geraniol were selected as the water-soluble mimetics of the natural post-translational modifications of HBV/HDV components. We have demonstrated their ability to interact with the vital central hydrophobic pocket of HBV and showed a binding affinity improvement upon dimerization of the geraniol ligand. Higher affinity ligands may be developed into even more potent binders of the hydrophobic pocket using the outlined linker design, potentially exerting a pharmacological effect on HBV.[50]

Earlier works demonstrated that point mutations within the HBc can significantly affect HBV infectivity, particularly through disruptions in HBc interactions.[51–54] These mutations at the base of the spike and the groove between spikes highlight the importance of these regions in viral replication. Using our structural knowledge of the capsid, particularly the distances between the spikes, we designed peptide dimers with the ability to simultaneously bind to neighboring spikes on the same capsid or attach to two distinct capsids (**Supplementary Figure 5**). Our in vitro assays demonstrated that these peptide dimers display a robust affinity ranging from low micromolar to sub-micromolar levels (**Figure 3** and **Supplementary Table 2**). Specifically, the

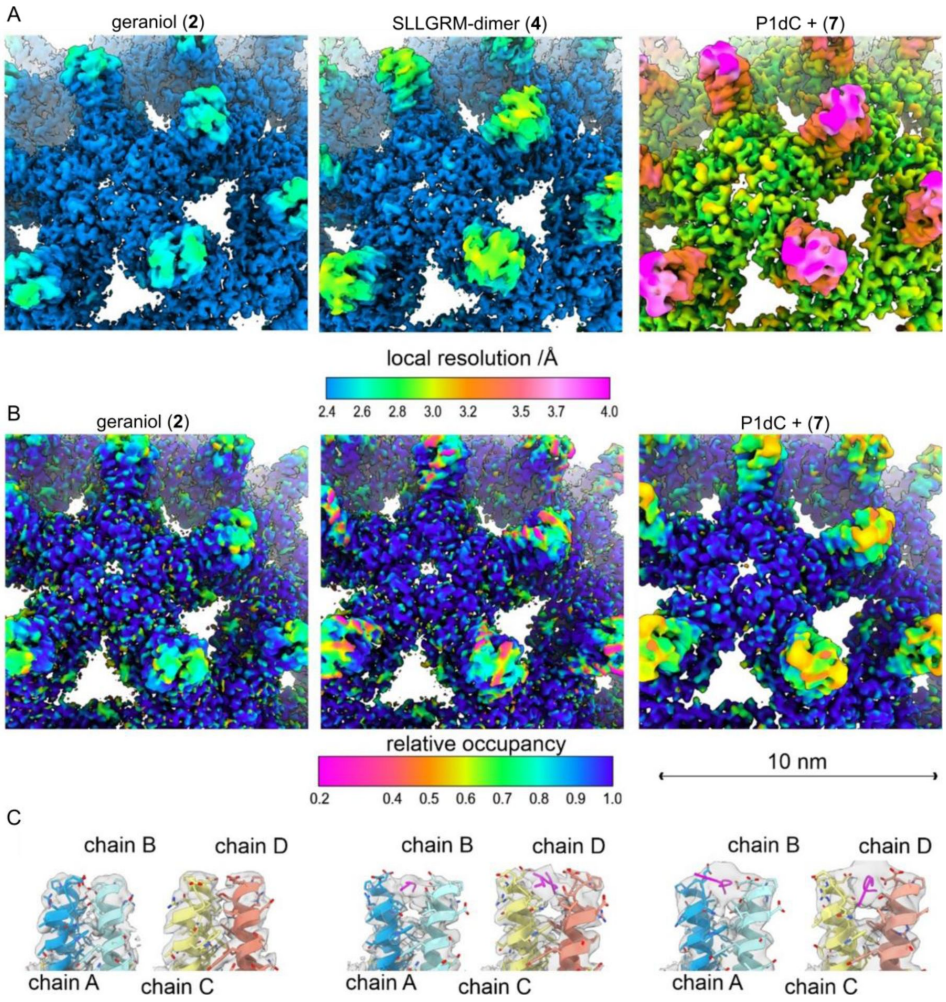

Figure 5.

Peptide dimers binding the spike tips.

Close up of the surface representation of the EM-maps of capsid-like particle (CLP) incubated with geraniol (**2**), with SLLGRM-dimer (**4**) and P1dC (**7**). (A) The surface of the map is colored according to the local resolution. The map of (**7**) has a lower overall resolution, which is consistent with the lower number of particles in the reconstruction (**Supplementary Table 4**). In all three maps the tips of the spikes are less well resolved than the capsid shell regardless of whether peptides are bound or not. This is in line with the general flexibility of the protruding spikes in HBc-CLPs.[37,48] (B) The surface of the maps is coloured according to the relative occupancy based on the grey value distribution as determined with OccuPy.[49] Low relative occupancy cannot be distinguished from local flexibility. As the tips of the spike are flexible, they show generally lower occupancy than the protein shell. Comparing the relative occupancies in samples incubated with (**4**) and (**7**) suggests a lower occupancy with (**4**) than with (**7**). (C) Fit between the model and the map (grey, translucent) at the tips of spikes. Binding of an (**4**) or of (**7**) splays the helices at the tips apart similar as previously reported for binding of a P2-monomer.[33] (**4**) binds to both quasi equivalent sites in contrast to SLLGRM-monomers, which binds only to the CD-dimer and does not show such a prominent splaying.[33] Geraniol binds at the center of the spikes and does not change the conformation at the tips of the spikes.

peptide dimer (P1dC) with sub-micromolar affinity (K_D=420 +/− 40 nM) is a promising candidate for a lead molecule for new a new class of CAMs. The peptide dimer, but not its scrambled dimeric counterpart, induced HBc aggregation in live mammalian cells expressing HBc. An effect resembling the aggregation observed after a treatment with the classical CAM HAP.[55]

An intriguing possibility would be that the spike and hydrophobic pocket interact or influence each other when binding different ligands. Molecular dynamics simulations reveal notable flexibility in HBV capsids, suggesting that structural asymmetry might impact ligand binding. Structural analysis of the HBV capsid shows that while P2 peptide binding to the capsid spikes increases flexibility, while exerting a minimal impact on the underlying hydrophobic pocket. However, TX100 binding within the hydrophobic pocket influences the spike tips by flipping Phe97, whereas geraniols bound within the same pocket do not induce this change, indicating that this interaction is ligand-specific. Nevertheless, simultaneous application of spike binders and hydrophobic pocket ligands that modify spike conformation may offer valuable structural and functional insights into HBV capsids.

An intriguing possibility would be that the spike and the hydrophobic pocket could interact or exert an effect on each other upon binding various ligands. Molecular dynamics simulations revealed significant flexibility of the HBV capsids and suggested that structural asymmetry may affect ligand binding.[56–58] HBV capsid structural analysis showed that P2 peptide binding to the capsid spikes, increases flexibility[33] while exerting a minimal impact on the hydrophobic pocket beneath. However, TX100 binding to the hydrophobic pocket affected the spike tips, by flipping Phe97[31] in the pocket, but the geraniols resolved within the hydrophobic pocket did not flip Phe97, thus suggesting that this cross-talk is ligand-specific. Nevertheless, a simultaneous application of spike binders and hydrophobic pocket ligands able to affect the spike conformation may provide valuable structural and functional insights on HBV capsids. While our results are highly encouraging, application in complex organisms may require alternative delivery methods, investigation of HBV proliferation in infection models, and further study of immunogenicity and stability. Future studies should thoroughly assess the cytotoxic potential of peptide-induced HBc aggregation to determine any adverse effects at the cellular level, which will be crucial for evaluating the therapeutic potential of these compounds. Long-term cytotoxicity studies on cellular viability are essential to optimize these binders for clinical applications. Although our study targets two ligand-binding pockets on the capsid surface, a direct effect on HBV infectivity remains to be demonstrated. Prior mutational data, however, suggest that even minor perturbations, such as ligand binding, could mimic deleterious mutations and impair viral function. This study's insights into the unexplored pharmacological potential of these binding pockets and the compounds targeting them may lead to the development of new agents that impact viral capsids. Unlike classical CAMs, the peptide dimers exhibit a different mechanism of action and may act synergistically with CAMs or other antivirals. Further biological investigations will clarify the antiviral potential, applicability, and potency of compounds targeting the non-HAP binding pockets.

Materials and Methods

Unless otherwise noted, all resins and reagents were purchased from IRIS biotechnologies or Carl Roth and used without further purification. All solvents were HPLC grade. All water-sensitive reactions were performed in anhydrous solvents under positive pressure of argon.

Peptide synthesis

The peptides were produced using standard solid phase peptide synthesis with Fmoc chemistry. Shortly, 2-chlorotrityl resin (1.6 mmol/g) was swollen in dry Dichloromethane (DCM) for 30 min., then, the desired amino acid (AA) (1eq) and the Boc-Gly-OH (1eq) with 4 eq. of dry N,N-

Diisopropylethylamine (DIEA) were added to the resin slurry. After overnight reaction at room temperature (RT) with agitation, the resin was capped with MeOH and washed with DCM and Dimethylformamide (DMF). For the synthesis of cysteinated peptides a 1% divinylbenzene Wang resin, preloaded with a 9-fluorenylmethyloxycarbonyl-Cysteine(Trityl)-OH [Fmoc-Cys(Trt)-OH] (0.4 mmol/g) was swollen in dimethylformamide (DMF) for 30 min. Then, regardless of the resin type, Fmoc was removed using 20% piperidine in DMF solution and the resin was washed with DMF and dichloromethane (DCM). After washes the peptide chain was elongated by adding the desired amino acid (AA, 3 eq.) with ethylcyanohydroxyiminoacetate (Oxyma, 3 eq.) and N,N'-diisopropylcarbodiimide (DIC, 3 eq.). Capping was done with N,N-diisopropylethylamine (DIEA, 50 eq.) and acetic anhydride (50 eq.) in N-methyl-2-pyrrolidone for 30 min. Coupling efficiency was monitored by measuring the absorption of the dibenzofulvene–piperidine adduct after deprotection. The peptide chain was elongated with further identical deprotection-conjugation cycles and after the completion the peptides were cleaved from the resin using a cocktail of 94% trifluoracetic acid (TFA), 3% H_2O, 3% Triisopropylsilane (TIPS), for 4 hours at RT. The peptides were precipitated in ice-cold ether and then purified with semi-preparative HPLC and analyzed by LC-MS, as described below.

5-(thio)-2-nitrobenzoate conjugation to the thiolated cell penetrating peptide (CPP)

A 10-mer oligoarginine peptide connected to a cysteine (C-RRRRRRRRRR) was reacted with 10 equivalents of 5,5-dithio-bis-(2-nitrobenzoic acid) in 1:1 DMF: 0.1 M phosphate buffer for 30 min with agitation at RT. Then the reaction mixture was directly injected in semi-preparative HPLC, purified and analyzed by LC-MS, as described below.

Purification and characterization of peptide-based probes

The compounds were purified from the crude reaction mix by reverse phase HPLC using a water acetonitrile gradient with 0.1% formic acid (FA). Semi-preparative HPLC was performed on Shimadzu Prominence equipped with a diode-array detector (DAD) system using a C18 reverse-phase column (Phenomenex Onyx Monolithic HD-C18 100×4.6 mm or Onyx Monolithic C18 100×10 mm). Purity and structural identity were verified using a DAD equipped 1260 Infinity II HPLC with a C18 reverse-phase column (Onyx Monolithic C18 50×2 mm), coupled to a mass selective detector single quadruple system (Agilent Technologies). Compounds analysed in ESI+ mode were run in a water-acetonitrile gradient with 0.1% formic acid (FA). Compounds analysed in ESI-mode were run in a 10 mM pH=7 ammonium bicarbonate – acetonitrile gradient.

Protein expression and purification HBc capsid like particles (CLPs)

The expression and purification of CLPs was done as previously described.[31] Shortly, the recombinant HBV core protein (HBc) was over-expressed in E. coli. and formed CLPs. CLPs were purified by fractionated ammonium sulfate precipitation followed by sucrose density gradient centrifugation. The major capsid type (ca. 95%) was formed by 240 subunits (Triangulation: T=4).

Isothermal titration calorimetry (ITC)

Samples (ca. 8 mL) of purified capsids were filtered (Rotilabo syringe filter with a pore size of 220 nm, Carl Roth GmbH Co. KG, Karlsruhe, Germany), dialysed against 1.4 L buffer A (40 mM HEPES, 200 mM NaCl, 1 mM $MgCl_2$, 1 mM $CaCl_2$, pH 7.5) using a dialysis membrane tube (Spectra Por Biotech cellulose ester tube, 1 MDa MWCO, Spectrum Laboratories, Inc., Rancho Dominguez, CA, USA). The dialysis was performed at 4 °C under gentle stirring for 16 h overnight. Next day, the dialysed sample was removed from the dialysis tube and concentrated in a centrifuge using a concentrator (30 kDa MWCO Spin-X UF 6 mL, Corning Inc., Corning, NY, USA). The concentrate was

filtered (centrifugal filter unit Ultrafree MC, pore size of 100 nm, Merck KGaA, Darmstadt, Germany) and the concentration determined by the Bradford assay (Roti Nanoquant, Carl Roth GmbH Co. KG, Karlsruhe, Germany).

The peptide dimers were dissolved in the buffer from the dialysis of the capsids. In this buffer, SLLGRM dimer and P2 dimer have solubilities of at >8 mM and the P1 dimer of >2 mM. 4 mM geraniol was titrated into a solution of 210 µM HBc.

A solution of 2 mM geranyl dimer was titrated into a solution 200 µM HBc. 1.6-2 mM solutions of DM were titrated into solutions with 90, 100 and 150 µM HBc, respectively.

Before filling the ITC cell and syringe, all samples were degassed for 10 minutes at 20 °C (ThermoVac, Malvern Panalytical, Malvern, Worcestershire, UK). Solutions of peptide dimers were titrated into solutions of capsids using a MicroCal iTC200 instrument (Malvern Panalytical, Malvern, Worcestershire, UK) according to the specifications in the **supplementary table 1**. The resulting thermograms and isotherms were processed and fitted by the Origin software supplied with the iTC200 instrument. The thermograms were integrated and the corresponding isotherms were fitted using a one site model. The peptide and geraniol dimers are bivalent and have 120 or 240 potential binding sites on CLPs, respectively. The two binding sites of peptide and geraniol dimers are not identical but very similar. This also true, for the binding sites on capsids, so the binding energetics of the dimers are very similar and are best represented by a one site model. All obtained thermodynamic parameters refer to concentrations of monomeric HBc. All ITC experiments were complemented with control experiments where solutions of peptide dimers were titrated into the dialysis buffer.

Turbidity assay

All peptides were dissolved in buffer A (40 mM HEPES, 200 mM NaCl, 1 mM $MgCl_2$, 1 mM $CaCl_2$, pH 7.5) and the capsid solutions were filtered once (centrifugal filter unit Ultrafree MC, pore size of 100 nm, Merck KGaA, Darmstadt, Germany). The concentrations of the P1, P2 and SLLGRM dimers were varied between 0.1-100 µM and the concentration of HBc was kept constant at 10 µM for the P1 and P2 dimer and at 50 µM for the SLLGRM dimer. All experiments were performed using a standard photometer (GENESYS™ UV/VIS spectral photometer, Thermo Fisher Scientific, Hillsboro, OR, USA) at RT and at a wavelength of 350 nm using disposable UV transparent cuvettes (SARSTEDT AG & Co. KG, Sarstedtstraße 1, 51588 Nümbrecht/Germany).

Cryogenic grid preparation of capsids in complex with peptid-dimers

In a plasma cleaner (model PDC-002. Harrick Plasma, Ithaca, NY, USA) holey carbon grids (R1.2/1.3, 300 mesh Cu grids, Quantifoil Micro Tools, Jena, Germany) were made hydrophilic by plasma cleaning. This was done at a pressure of 29 Pa for 2 minutes using ambient air as plasma medium at “medium power” of the instrument. Solutions of purified HBc (200 µM) in complex with the P1dC- and the SLLGRM-dimer (each 400 µM) were prepared in buffer A. After the end of ITC experiment with geraniol and HBc (**Figure 2**), a sample from the cell of the ITC instrument was retrieved and used for freezing grids. 3.5 µl aliquots of each sample were applied onto the grids. For plunge freezing of grids ethane was used as medium (liquefied by liquid nitrogen) with the help of a Vitrobot (mark IV, FEI Company, Hillsboro, OR, USA) using filter papers of Whatman (type 541). The Vitrobot had the following settings: no wait and drain times, 6 s of blot time, blot force of 25 and a nominal humidity of 100 %. The frozen grids were stored in liquid nitrogen for at least one night before being used for image acquisition.

Cryo-EM and image processing

Cryo-EM was done as previously described. [31] Shortly, movies were acquired with the software EPU on a Krios G3 electron microscope equipped with a Falcon III camera (Thermo Fisher Scientific, Hillsboro, OR, USA) in integrating mode at a magnification of 75,000 with an accelerating voltage of 300 kV. The total exposure was 40 $e^{-}/Å^2$ and was fractionated over 20 fractions. For HBc CLPs with bound P1dC, 3 movies were acquired per hole and one hole was acquired per stage position. For HBc CLPs with bound SLLGRM dimers or bound geraniol, at each stage position three movies were acquired per hole from the central hole and from the four closest neighboring holes. The different movie positions at the same stage position were centered with image shift. Movies were motion corrected, exposure weighted and averaged with MotionCorr2. **Figure S6a** shows representative corrected movie averages, which were imported to Relion for further processing. Each image shift position was treated as a different optics group in the subsequent image processing. Image processing was done with Relion 3.1 or Relion 4. As previously described [31] imposing icosahedral symmetry. At the end of the image processing with Relion (for CLPs with bound P1dC or SLLGRM-dimers), particle images were imported into CryoSparc 4.02 and were further refined with none uniform refinement [59], including global and local CTF refinement and Ewald's sphere correction. Final maps were filtered with deepemhancer, or B-factor sharpened (CryoSPARC "Sharpen" or "relion_postprocess"). The resolution of the final maps was estimated by Fourier-Shell-Correlation (FSC=0.143; after gold standard refinement) with "relion_postprocess" (**Figure S6**). Parameters of the image acquisition and the processing are summarized in **table S3**.

Modelling of Cryo-EM maps, refinement of PDB files and their validation

For modelling of the EM densities of HBc in complex with the peptide dimers the PDB file 7od6[33] was used as starting model. This model represents the asymmetric unit of the HBc capsids with T=4 packing. After slight modifications, the PDB model was fitted into the EM-map as a rigid body and refined iteratively by the software packages Coot[60] and Phenix[61] and validated by MolProbidity.[62] The resolution of the density at the tips of the capsids which we attributed to the binding segments of the peptide dimers was low. Therefore, these densities could only be modelled as poly-alanine chains. All figures showing EM-densities with or without the corresponding PDB models were prepared with Chimera.[63]

Cloning

Full length wild type (fl wt) HBc (genotype D; strain ayw; GenBank: V01460.1, MQLFHLCLIISCSCPTVQASKLCLGWLWGMDIDPYKEFGATVELSFLPSDFFPSVRDLLDTA SALYREALESPEHCSPHHTALRQAILCWGELMTLATWVGVNLEDPASRDLVVSYVNTNMG LKFRQLLWFHISCLTFGRETVIEYLVSFGVWIRTPPAYRPPNAPILSTLPETTVVRRRGRSPR RRTPSPRRRRSQSPRRRRSQSRESQC)[64] was cloned into the pEGFP-C2 vector (Clontech) using Gibson assembly[65] by replacing the gene sequence coding for eGFP. The vector and insert were amplified by PCR and purified by gel extraction (FastGene Gel/PCR Extraction Kit, Nippon Genetics Europe GmbH, Düren, Germany). The purified PCR products were assembled into a single plasmid construct using a home-made Gibson assembly reaction mixture. An aliquot of the reaction product was transformed into XL1 blue cells, plated onto LB-amp agar-plates and grown at 37 °C ON. Six colonies were used for the inoculation of 6 x 5 mL LB-amp medium. The cell cultures were grown under vigorous shaking in an incubator at 37 °C ON. Next day, the plasmid DNA was extracted from the cell cultures (FastGene Plasmid Mini Kit, Nippon Genetics Europe GmbH, Düren, Germany) and sequenced by Sanger sequencing (Microsynth Seqlab GmbH, Göttingen, Germany). A plasmid construct containing the correct gene sequence of HBc was used for endotoxin-free plasmid DNA preparation (NucleoBond Xtra Midi EF, Macherey Nagel GmbH & Co. KG, Düren, Germany).

HEK293 cell cultures and transfection

HEK293 cells were cultured in DMEM (GIBCO), supplemented with GlutaMax and pyruvate (GIBCO), 10% fetal bovine serum (GIBCO) and 1% Penicillin/Streptomycin (Sigma) at 37°C and with 5% CO_2. The cells were plated on 0.15 mm thick 18 mm glass coverslips coated with 35 µg/ml Poly-D-Lysine in a 12-well plate and were transfected with the cloned 1 µg plasmid DNA per coverslip using PEI (Polyethylenimine). The transfection was performed at 60-80% confluence. Shortly before transfection the medium was changed to fresh DMEM. The DNA was added to 100 µl DMEM without additives and mixed, 4 µL fresh PEI (1 mg/mL) was added, mixed immediately and incubated for 20 min at RT. The transfection mix was pipetted drop-wise on cells while swirling, and incubated overnight. The medium was changed to fresh DMEM with 2% FBS after 12-24 hours, and on the following day the cells were used for live assays, then fixed and stained.

Cell assays and immunocytochemistry

Live HEK293 cells expressing HBc were incubated in DMEM with 10 µM P1dC and with 10 µM of the scrambled version of the peptide, both peptides in-situ activated with the reactive CPP. After 1-hour incubation at 37°C the treated and the untreated live HEK293 cells expressing HBc and the untransfected HEK293 cells were washed and fixed with 0.1 M sodium phosphate buffer pH 7.4 containing 4% paraformaldehyde (EM grade, Polysciences) and 1% sucrose for 10-20 min at 37°C. After three rinses in phosphate buffered saline (PBS), the cells were permeabilized with 0.1% Triton X-100 in PBS for 10 min at RT, rinsed again and blocked for 1 h in PBS with 3% bovine serum albumin (BSA). Then, primary mAb16988 (#6B9780, MilliporeSigma) and secondary DyLight650 (#84545, Invitrogen) antibodies were applied sequentially with 1:500 dilution in blocking solution for 1 hour.

Wide field fluorescence microscopy

The coverslips with the cell samples were inserted in an imaging chamber (Ludin Chamber Type 1, Life Imaging Services) and imaged in PBS. The measurements were taken from distinct samples with a sample size ≥ 2, for each group. A series of images, used to generate the datapoints, were acquired from different regions of the sample, each region having a distinct group of cells.

The samples were imaged on an inverted Leica DMI6000B microscope with a 100x oil-immersion objective (NA 1.49) using a Leica DFC9000 GTC VSC-05760 sCMOS camera (16-bit, image pixel size: 130 nm). The 628/40 excitation and 692/40 emission filter was used for DyLight650, 10 images were acquired at a frame rate (exposure time) of 100 ms and constant illumination intensity to ensure comparability. n≥10.

Automated Solid-Phase Peptide Synthesis

µSPOT peptide arrays [66] were synthesized using a MultiPep RSi robot (CEM GmbH, Kamp-Lindford, Germany) on in-house produced, acid-labile, amino-functionalized, cellulose membrane discs containing 9-fluorenylmethyloxycarbonyl-β-alanine (Fmoc-β-Ala) linkers (average loading: 130 nmol/disc – 4 mm diameter). Synthesis was initiated by Fmoc deprotection using 20% piperidine (pip) in dimethylformamide (DMF) followed by washing with DMF and ethanol (EtOH). Peptide chain elongation was achieved using a coupling solution consisting of preactivated amino acids (aas, 0.5 M) with ethyl 2-cyano-2-(hydroxyimino)acetate (oxyma, 1 M) and N,N'-diisopropylcarbodiimide (DIC, 1 M) in DMF (1:1:1, aa:oxyma:DIC). Couplings were carried out for 3 × 30 min, followed by capping (4% acetic anhydride in DMF) and washes with DMF and EtOH. Synthesis was finalized by deprotection with 20% pip in DMF (2 × 4 µL/disc for 10 min each), followed by washing with DMF and EtOH. Dried discs were transferred to 96 deep-well blocks and treated, while shaking, with sidechain deprotection solution, consisting of 90% trifluoracetic acid (TFA), 2% dichloromethane (DCM), 5% H_2O and 3% triisopropylsilane (TIPS) (150 µL/well) for 1.5 h at RT. Afterwards, the deprotection solution was removed, and the discs were solubilized

overnight (ON) at RT, while shaking, using a solvation mixture containing 88.5% TFA, 4% trifluoromethanesulfonic acid (TFMSA), 5% H_2O and 2.5% TIPS (250 µL/well). The resulting peptide-cellulose conjugates (PCCs) were precipitated with ice-cold ether (0.7 mL/well) and spun down at 2000 × g for 10 min at 4 °C, followed by two additional washes of the formed pellet with ice-cold ether. The resulting pellets were dissolved in DMSO (250 µL/well) to give final stocks. PCC solutions were mixed 2:1 with saline-sodium citrate (SSC) buffer (150 mM NaCl, 15 mM trisodium citrate, pH 7.0) and transferred to a 384-well plate. For transfer of the PCC solutions to white coated CelluSpot blank slides (76 × 26 mm, Intavis AG), a SlideSpotter (CEM GmbH) was used. After completion of the printing procedure, slides were left to dry ON.

Peptide Microarray-Binding Assay

The microarray slides were blocked for 60 min in 5% (w/v) skimmed milk powder (Carl Roth) phosphate-buffered saline (PBS; 137 mM NaCl, 2.7 mM KCl, 10 mM Na_2HPO_4, 1.8 mM KH_2PO_4, pH 7.4). After blocking, the slides were incubated for 15 min with 55 nM (monomer equivalent) of HBc in the blocking buffer, then washed 3× with PBS. HBc was detected with a primary 1:2500 diluted mAb16988 (anti-hepatitis B virus antibody, core antigen, clone C1-5, aa 74-89, MilliporeSigma, Darmstadt, Germany) and a secondary 1:5000 diluted HRP-coupled Anti-mouse antibody (31,430, Invitrogen). The antibodies were applied in blocking buffer for 15 min, with three PBS washes between the antibodies and after applying the secondary antibody. The chemiluminescent readout was obtained using SuperSignal West Femto maximum sensitive substrate (Thermo Scientific GmbH, Schwerte, Germany) with a c400 Azure imaging system (lowest sensitivity, 90 s exposure time).

Binding intensities were quantified with FIJI[67] using the “microarray profile” plugin (OptiNav Inc, Bellevue, WA, USA). The raw grayscale intensities for each position were obtained for the left and right sides of the internal duplicate on each microarray slide, n = 3 arrays in total. Blank spots were used to determine the average background grayscale value that was subtracted from the raw grayscale intensities of non-blank spots. Afterward, the spot intensities were normalized to the average grayscale value of the 14 replicates of peptide binder P1 (“MHRSLLGRMKGA”).

Supplementary Figures

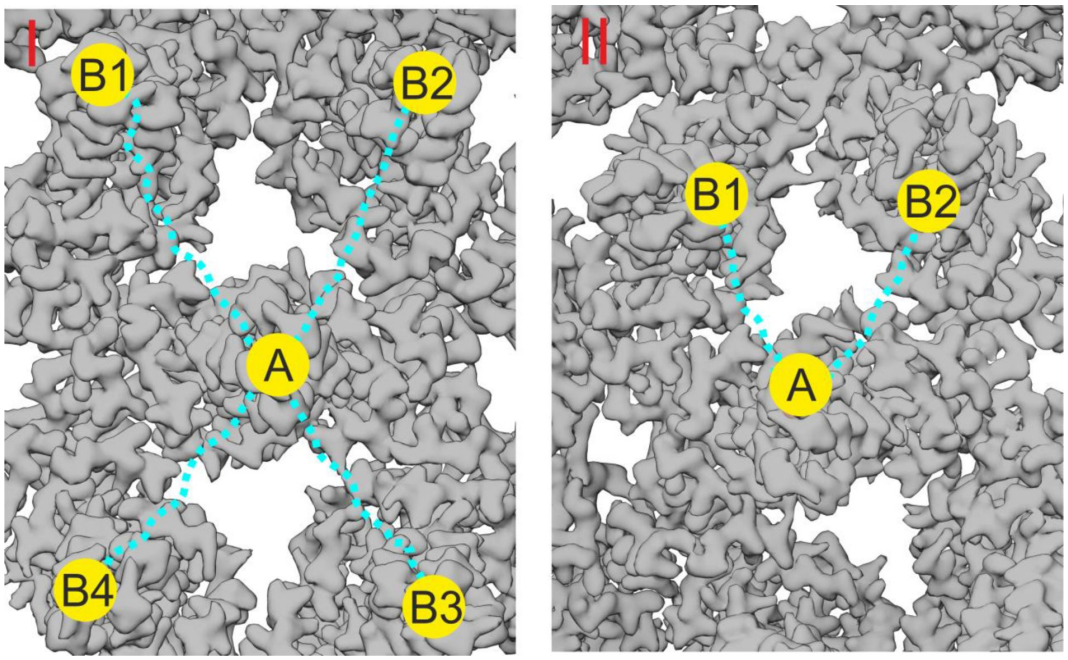

Supplementary Figure 1

Rational design of multivalent binders.

This figure illustrates the rationale behind the design of the PEG linker length in the peptide- and geraniol-dimers. The binding site A, where the peptide or geraniol dimer binds, is located at the tip of a capsid spike or in a hydrophobic pocket (depicted as a yellow circle). The possible additional interactions of the dimers are shown as yellow circles labeled B1, B2, B3, and B4. The PEG linker, depicted as a dotted blue line, has been carefully chosen to allow simultaneous binding between two opposing sites. (I) The distance between the tip of a "central" capsid spike (A) and the surrounding four spikes (B1, B2, B3, and B4) is approximately 6 nm (60 Å). The PEG linker, with a length of about 8 nm (80 Å), was selected to provide flexibility and ensure the dimer can potentially bridge two adjacent spike tips, optimizing binding avidity by enabling interaction with any combination of the adjacent spikes. (II) For geraniol dimers, the hydrophobic pockets are separated by a distance of approximately 4 nm (40 Å), and the designed PEG linker (~3.8 nm or 38 Å) was chosen to match this distance, allowing for optimal interaction with two pockets in close proximity.

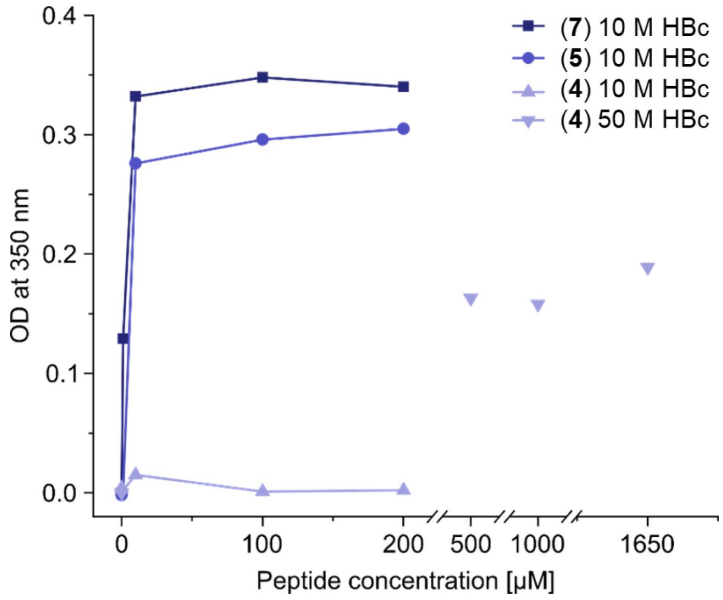

Supplementary Figure 2.

High turbidity is observed upon addition of HBc binding dimers to HBc solution.

Assessment of turbidity of capsid solutions induced by peptide dimers. The optical densities (OD) of HBc solutions (10 or 50 μM) with and increasing peptide-dimer concentrations were measured at a wavelength of 350 nm and plotted against peptide-dimer concentrations. All peptides showed increased turbidity with increasing concentrations, with P1 (**7**) and P2 (**5**) dimers inducing turbidity at low micromolar concentrations, while the SLLGRM dimer (**4**) induced turbidity at high micromolar concentrations.

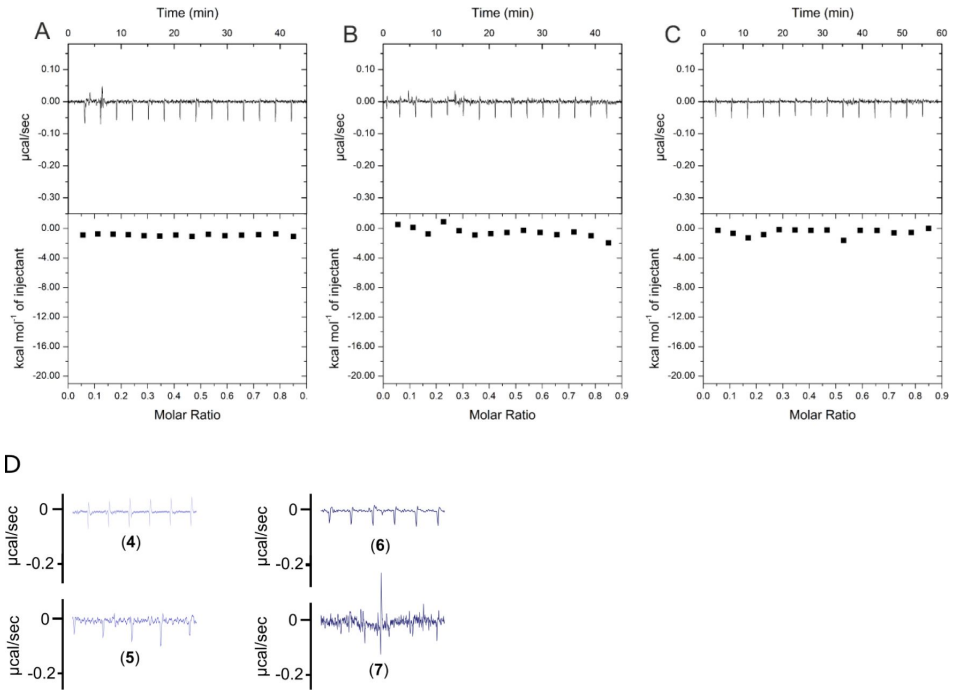

Supplementary Figure 3.

scrP1dC does not interact with HBc.

A) 0.1 mM solution of the scrP1dC-dimer (scrambled version of the P1dC-dimer) was titrated into a solution of 0.025 mM HBc. B and C) 0.1 mM solutions of scrP1dC-dimer and P1dC-dimer were titrated into buffer A as additional controls. In all cases no heat change was examined, validating the lack of HBc – scrambled peptide interaction and excluding residual binding interactions from the handle or linker. D) Heat fluctuations from **Fig3B** on identical y-axis scaling.

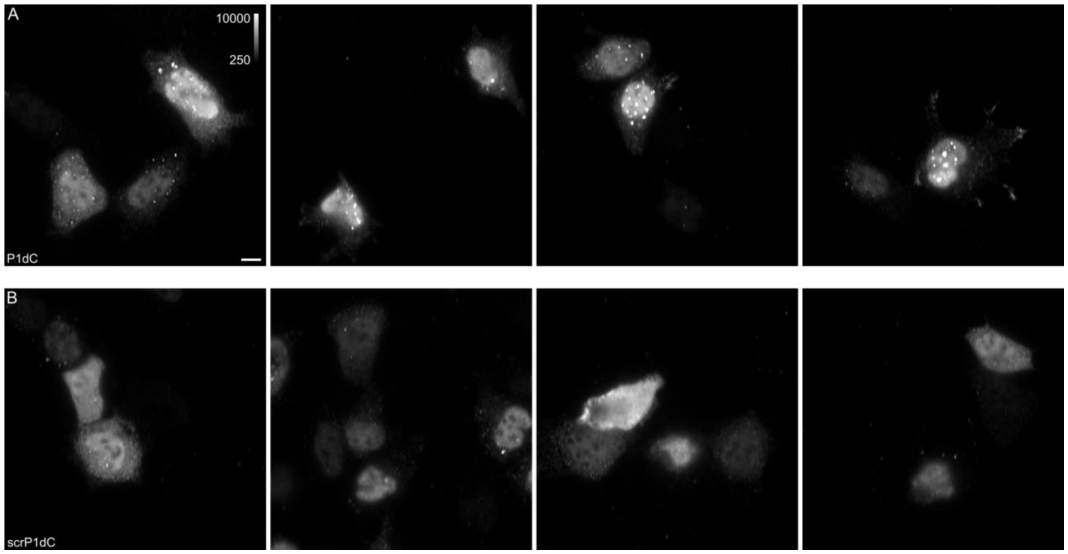

Supplementary Figure 4.

HBc aggregates appear after treatment with P1dC.

Live HEK293 cells expressing HBc were treated with either P1dC or with the scrambled (scr) P1dC analogue together with the cell penetrating peptide. After treatment, the live cells were fixed and labelled with HBc Antibody and a secondary DyLight650 conjugated antibody (1:500). The imaging showed HBc aggregates in P1dC treated cells (A), while scrP1dC treated cells showed little to none aggregates (B). All images shown with identical grayscale range. Scale bar 10 µm.

Peptide-dimers have a complex interaction pattern with capsids

For an adequate interpretation of the ITC experiments it is important to note that in the presence of peptide dimers the asymmetric unit (homo-tetramer consisting of 2 HBc dimers) of HBc capsids (T =4 particles) has at least several distinct states which are in dynamic equilibria (**Supplementary Figure 5**). If the concentration of HBc is kept constant, the concentration of each state will depend on the concentration of the peptide-dimer. In this case the stoichiometry of the peptide dimers' binding to HBc is 0.25 (1:4) - 0.5 (1:2). The 60 asymmetric units of a single capsid will have a mixture of all possible states depending on the concentration of the peptide-dimer. At low peptide concentrations (below N = 0.25), S1 will be energetically favored and at high peptide concentrations (above N = 0.25) S4 will be favored. Within a capsid there are an astronomical number of different states and interactions. For example, a capsid in S4 can interact with nearby capsids in S0, S2 and S3 and cross-link them.

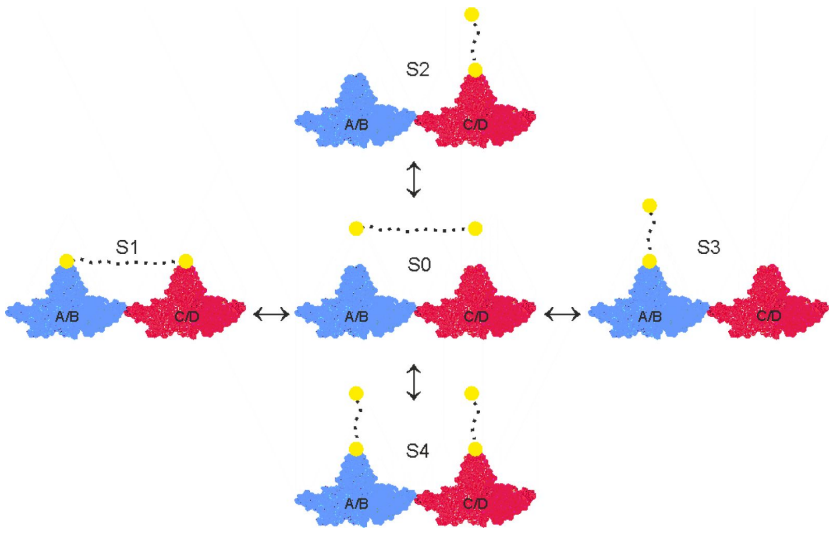

Supplementary Figure 5

Overview of equilibria between the asymmetric unit of HBc and peptide-binders.

The asymmetric unit of HBc capsids (T =4) consists of a tetramer which is composed of the A/B (closest to the 5-fold symmetry axes in the icosahedron) (in blue) and the C/D-dimer (closest to the 3-fold symmetry axes) (in red). The peptide moiety of the dimers is depicted as yellow filled circles connected by a flexible PEG linker symbolized as a dotted line. Peptide dimers interact with the asymmetric unit in 4 different states (S1, S2, S3 and S4). The concentration of every state is dictated by the energetics of the respective state and the concentration of the peptide-dimer. At low concentrations, S1 and the possible degenerative permutations could be expected to be favored and at high concentrations S4. For the sake of simplicity, only a single (abstract) asymmetric unit is depicted here which represents capsid with 60 asymmetric units.

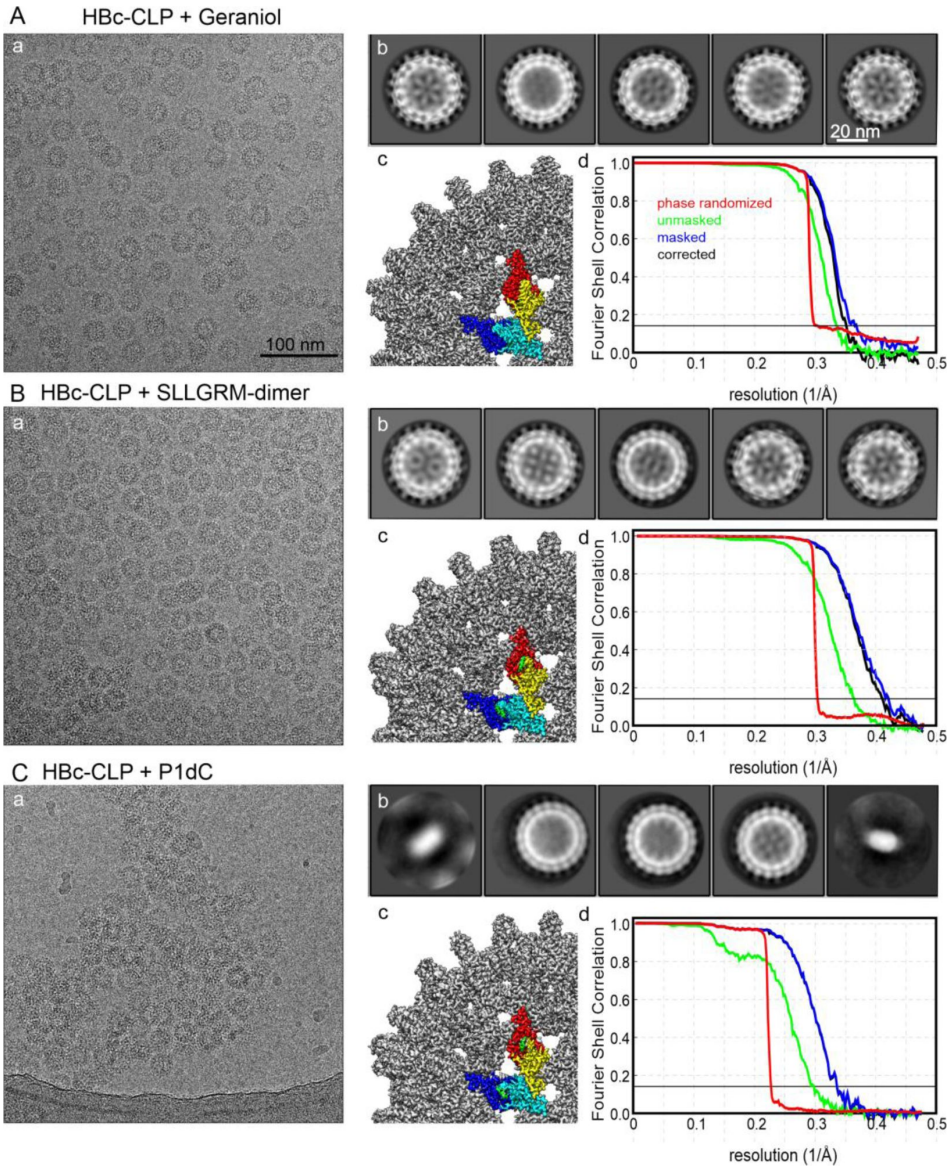

Supplementary Figure 6

Electron microscopy and image processing of HBc-CLPs with binders: A) CLPs with bound Geraniol, B) HBc-CLPs with bound SLLGRM-dimer and C) HBC-CLPs with bound P1dC

A) shows a representative micrograph. All micrographs are shown at the same scale as indicated in Aa; B) shows the 2D-Class averages of the 5 most populated classes after automated template picking. All class averages are shown at the same scale as indicated in Ab; C) shows a close-up of the surface representation of the final map after post-processing with relion (filtered by Fourier Shell Correlation (FSC), B-factor sharpened). One unit cell is colored according to the density covered by the model (HBc chains A, B, C, D in blue, cyan, yellow and red respectively, and binders (geraniol, SLLGM and P1 in green); D) Fourier Shell Correlation plot of the final map. FSC=0.143 is marked by a thin, solid line. Green curve: FSC between unmasked half-maps, blue curve: FSC between masked half-maps; red-curve FSC between phase-randomized masked half-maps, black curve: FSC corrected for the contribution of the mask.

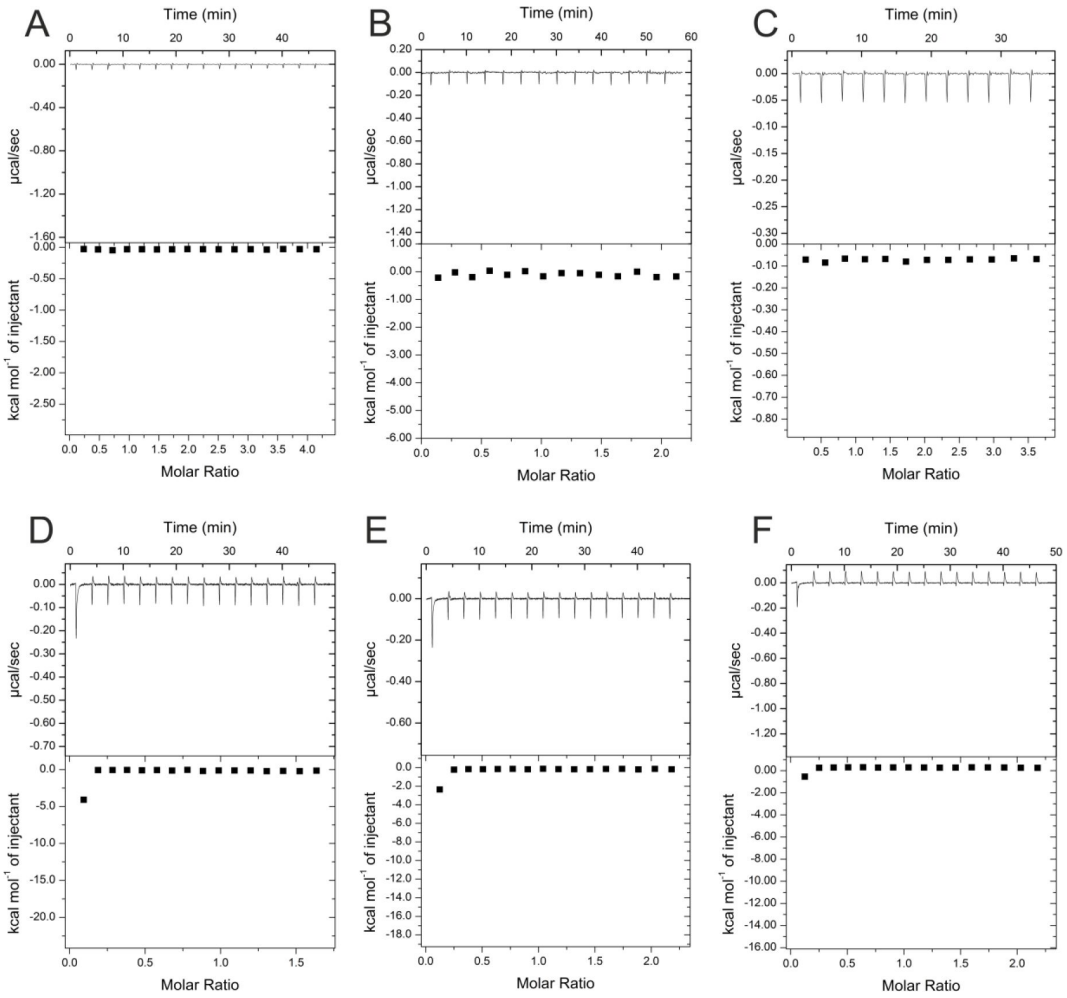

Supplementary Figure 7.

Control titrations of substances used for ITC experiments.

All substances were dissolved in buffer A and titrated into buffer A as a control for experiments where equal concentrations of these substances were titrated into solutions of HBc (see **Figures 2** and **3** in the main text). A) 4 mM geraniol, B) 2 mM geraniol dimer, C) 1.7 mM DM, D) 0.3 mM P1d, E) 0.5 mM P2d and F) 1.5 mM SLLGRM dimer. X and Y axes are scaled differently in the panels.

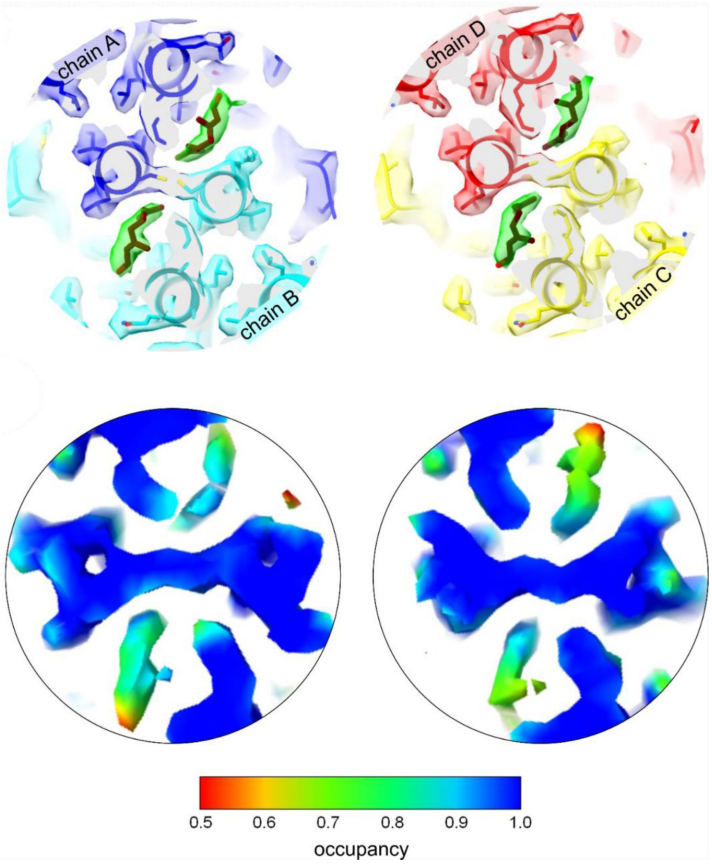

Supplementary Figure 8.

Geraniol binding mode to the hydrophobic pocket at the base of the capsid spike.

(A) Model of the CD-dimer (yellow, red) with bound geraniol (purple) inside the EM-map (transparent). The density accounted by geraniol is shown in blue. Right: close-up of the hydrophobic pocket with residues labelled in the vicinity of geraniol and at the entrance of the pocket. Residues P5, L60 and K96 are implicated with naturally occurring envelopment phenotypes. Close-up of the quasi-equivalent hydrophobic pockets with bound geraniol. (B) Slice of the EM-map with fitted model: The slice shows the center of the two quasi-equivalent spikes with the fitted models of Geraniol in brown. One Geraniol molecule is bound to each of the quasi-equivalent sites. The surface of the EM-map is transparent and coloured according to the chains. For clarity the density attributed to Geraniol is highlighted in green (colour blob option of Chimera[68]). Geraniol binds to the same site as Triton X100[31] but does not change the rotamer conformation of F97. Binding of geraniol is not linked to conformational changes in the HBc-dimers. (C) Slices of the EM-map at the centre of the spikes shown above. The surface of the map is coloured according to the relative occupancy estimated with "OccuPy"[49] based on the grey value distribution. The relative occupancies at the geraniol moiety are somewhat lower than the surrounding protein. Considering that flexibility and occupancy have a similar effect on the grey value distribution, the geraniol has an increasing flexibility towards the outside of the pocket and has at least 80-90% occupancy at the interior of the pockets. The colour key for the relative occupancy is shown below.

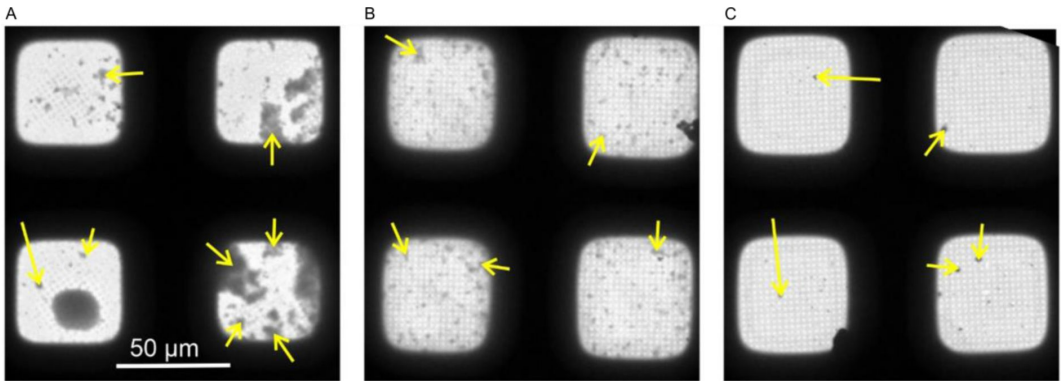

Supplementary Figure 9.

Cryo-EM confirms strong capsid aggregation with peptide dimers.

Low magnification cryo-EM images of CLPs + P1dC (**7**) (A), (B) CLPs + SLLGRM-dimer (**4**) and (C) CLPs + geraniol (**2**). The micrographs are part of the grid-atlas of the respective data acquisition. Each image shows 4 meshes of the respective grid atlas at a similar ice thickness. For representation, the images were aligned to show a similar orientation of the meshes. CLP aggregates are seen as dark speckles (yellow arrow). The size of the aggregates is largest in P1dC-treated samples, while aggregates are frequent and smaller in samples treated with SLLGRM-dimer. Geraniol treated samples have very few aggregates which are generally smaller than 1 µm.

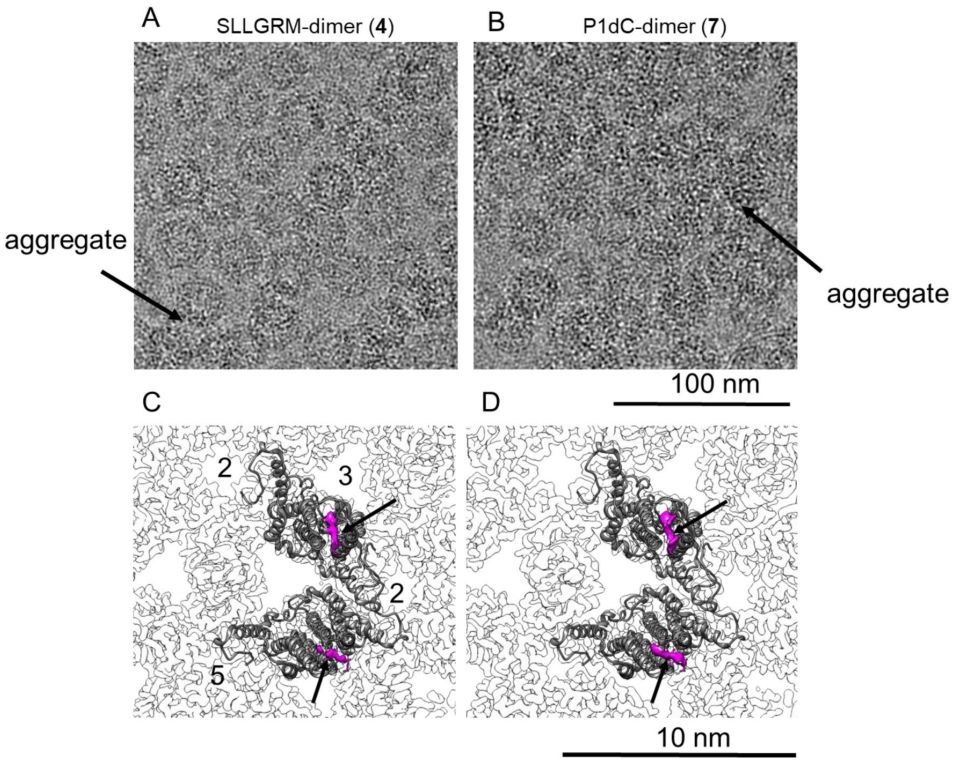

Supplementary Figure 10.

Nanoscale resolution of the dimer binding sites by Cryo-EM.

HBc capsids with bound SLLGRM-dimer (**4**) or P1dC-dimer (**7**) imaged by electron cryo-microscopy. (A) and (B) show selected areas of micrographs of CLPs treated with (**4**) or with (**7**). One exemplary aggregate of multiple HBc capsids is indicated by an arrow in each micrograph. (C) and (D) show close-ups of the asymmetric unit of HBc capsids with bound SLLGRM dimers or with bound P1dC. Models of a single asymmetric unit consisting of two HBc dimers is fitted into the asymmetric unit. Both maps show a density at the tips of the spikes (arrow) that accounts for approximately six amino acids of the peptide-dimer. The flexible linker between the peptides was not resolved. The position of the symmetry axes of the icosahedral capsid is labelled with numbers in (C).

Supplementary Tables

Acknowledgements

H.M.M. acknowledges the support of the Junior Group Leader program of the Rudolf Virchow Center, University of Würzburg the excellent ideas programme of the JMU and support through DFG MA6957/1-1. BB acknowledges support for this project by the DFG (BO1150/17-1). Electron microscopic data were acquired at the cryo-EM facility in Würzburg funded by the German Research Foundation (DFG – projects 359471283, 456578072, 525040890).

Appendix 1. Chromatographic and mass spectrometric analytical data

Supplementary Table 1.

ITC200 specifications

ITC200 instrument's specifications used for the interaction analysis between peptides and capsids.

Number of injections	**14-16**		
Cell Temperature (°C)	20		
Reference power (µCal/s)	11		
Initial delay (s)	60 -180	**Injection parameters:**	
Syringe concentration (mM)	0.1 – 1.5 for peptide dimers 1.6 – 2 mM for DM 4 mM for geraniol 2-3 mM for the geraniol dimer	**Volume (µL)**	2.5 – 2.8
Cell concentration (mM)	0.025 - 0.15 HBc	**duration (s)**	5 – 5.6
Stirring speed (rpm)	600	**Spacing (s)**	180/240
Feedback mode	high	**Filter period (s)**	5/1
First injection	No first injection	**Cell volume (mL)**	0.200

Supplementary Table 2.

Thermodynamic parameters of HBc capsids interactions.

Summary of thermodynamic parameters obtained by ITC experiments using the peptide dimers and fl wt HBc capsids. In case of the P2 dimer the deviations represent deviations of fit since only one ITC experiment was performed. N represents stoichiometry.

Peptide dimer	**N**	**K_a $\frac{1}{M}$**	**K_D µM**	**ΔH $\frac{cal}{mol}$**	**ΔS $\frac{cal}{mol \times K}$**	**Repeats**
SLLGRM dimer (4)	0.15 ±0.02	210000 ±30000	4.9 ±0.7	-25 ±3	-62 ±10	5
P2 dimer (5)	0.157 ±0.014	500000 ±110000	1.9 ±0.4	-30 ±3	-76 ±n/a	1
P1 dimer (6)	0.19 ±0.04	6000000 ±6000000	0.3 ±0.2	-26 ±4	-58 ±15	4
P1dC (7)	0.196 ±0.005	2490000 ±230000	0.42 ±0.04	-21.7 ±0.6	-45 ±2	3
DM (1)	1.1 ±0.1	8000 +/-2300	133 ±38	-2.5 ±0.7	9.2 ±2.6	3
Geraniol (2)	1.01±0.036	10600+/-900	94.3 ±7.9	-4.3 ±0.2	3.9 ±n/a	1
Geranyl dimer (3)	0.236±0.037	16000+/-2000	62.5 ±7.9	-14.4 ±2.6	-30 ±n/a	1

	M	H	R	S	L	L	G	R	M	K	G	A
A	28.29±8.01	29.76±2.22	98.61±16.96	10.15±3.11	8.31±4.76	5.55±2.14	5.9±0.71	55.58±22.38	11.72±0.47	57.66±14.23	16.98±4.54	24.35±6.34
C	19.43±7.82	22.13±2.95	34.85±8.45	4.47±1.85	6.67±3.89	4.78±1.94	4.24±1.06	7.42±4.58	4.5±1.31	15.67±8.52	7.61±3.77	8.92±3.67
D	41.36±8.62	40.58±9.04	121.37±4.42	13.66±1.88	5.77±3.05	4.61±2.27	4.92±1.9	11.37±3.38	3.94±1.44	42.48±12.79	33.5±8.31	15.97±5.07
E	27.72±9.75	74.46±26.92	174.74±10.87	22.15±6.15	5.87±2.73	5.12±2.83	5.19±1.01	125.85±26.07	12.24±4.47	214.54±10.27	69.7±11.56	20.01±4.57
F	20.39±7.92	30.83±6.54	82.39±11.3	18.17±1.59	5.37±2.17	4.32±2.34	5.01±1.13	71.47±10.55	97.92±44.3	36.67±6.8	19.25±4.34	8.11±1.93
G	23.03±7.29	31.38±5.87	74.75±12.89	17.14±2.46	4.93±1.54	4.03±2.56	24.35±6.34	14.7±2.45	6.91±2.98	25.3±4.33	24.35±6.34	11.49±3.45
H	21.14±7.86	24.35±6.34	59.98±9.75	18.74±4.3	7.24±1.91	3.47±1.98	4.85±2.52	11.25±3.78	10.4±2.62	29.27±9.36	15.37±4.17	14.05±3.24
I	20.6±5.3	29.76±6.65	53.52±3.88	13.52±7.8	17.48±1	3.5±1.82	4.4±2.08	58.16±15.17	131.06±32.41	160.1±29.36	45.69±10.05	21.72±4.15
K	19.65±8.04	21.14±3.01	36.94±6.51	10.49±4.75	11.69±1.09	2.88±1.77	4.32±2.52	14.46±4.98	13.67±3.91	24.35±6.34	16.66±2.36	8.21±1.39
L	19.9±4.19	37.55±5.86	46.32±6.64	9.58±3.9	24.35±6.34	24.35±6.34	4.13±2.54	17.18±6.39	112.4±19.28	48.01±12.59	48.89±11.32	15.77±1.8
M	24.35±6.34	38.05±1.54	88.79±10.41	11.34±2.2	6.32±4.08	2.28±1.77	3.93±2.27	38.17±15.55	24.35±6.34	45.9±11.89	53.16±13.45	13.2±0.38
N	23.46±4.29	32.64±10.78	60.64±4.04	9.95±2.75	4.77±2.71	3.21±1.78	7.19±2.82	12.72±6.84	8.52±1.93	23.98±7.23	24.2±9.29	14.78±1.73
P	25±4.8	30.7±7	53.35±12.52	15.29±3.14	4.99±2.49	3.64±2.19	5.33±2.27	13.43±9.39	7.96±1.94	7.21±2.41	14.45±7.15	19.42±3.2
Q	36.28±2.46	33.37±9.32	101.47±27.8	11.96±2.86	5.57±2.33	4.53±2.12	5.56±1.75	24.98±11.5	6.52±1.19	33.79±12.74	20.91±8.74	11.9±0.68
R	41.77±9.55	20.21±3.8	24.35±6.34	10.02±3.41	4.77±1.77	2.87±2.06	2.58±1.79	24.35±6.34	4.88±2.05	14±3.77	8.84±4.07	7.41±3.45
S	44.06±13.76	26.62±5.31	78.81±31.78	24.35±6.34	5.93±1.14	4.59±2.82	3.33±1.67	144.71±41.04	4.77±2.02	54.06±11.98	25.76±5.27	33.45±7.32
T	46.27±11.34	33.45±7.37	98.92±36.7	18.1±4.05	7.5±1.55	5.14±1.93	3.03±1.87	119.43±39.05	11.7±3.32	105.84±15.55	24.42±3.19	22.6±4.5
V	40.77±6.59	23.28±3.08	61.38±14.66	10±3.75	10.25±3.18	5.03±1.89	3.44±1.73	121.7±34.59	62.83±13.91	75.04±18.53	25.35±6.34	25.41±6.81
W	32.39±4.15	25.47±2.95	24.52±6.54	6.66±3.12	4.46±2.14	3.82±1.21	2.03±1.88	9.3±2.67	8.41±3.84	9.39±2.16	5.97±2.03	5.68±1.13
Y	31.23±0.54	52.65±4.23	52.64±8.14	11.07±6.3	5.88±3.02	5.67±0.82	3.91±2.79	38.44±2.9	12.1±4.48	14.09±3.83	11.9±2.42	10.38±2.03

Supplementary Table 3

Microarray positional scan data.

Obtained raw greyscale values from P1 full positional scan in μSPOT format. Each box corresponds to a single point variation of the P1 peptide sequence (horizontal) as indicated in the first column. The raw intensity values presented here were used for calculating the fold intensity change of each point variation against the wildtype sequence. Data are presented as mean of n=3 microarray slides with standard deviation.

Data Acquisition and Image Processing

	HBc CLPs + Geraniol (2)	HBc CLP+ SLLGRM dimer (4)	HBc CLP + P1dC (7)
Microscope	Krios G3 300 kV, with Falcon III camera in linear mode		
Illumination	Spot 5 nano probe; C2 aperture =70 µm; beam diameter 1 µm,		
Imaging	Magnification: 75000 x, calibrated Pixel size: 1.064 Å/Px, objective aperture: 100 µm		
Exposure	Total exposure = 40 $e^-/Å^2$ in 20 fractions; exposure time: 2.6-3.2 s		
Targeted underfocus	600-1400 nm		
Movies per stage position	15 in 5 holes	15 in 5 holes	3 in 1 hole
Movies	4875	4956	2784
Template picked Particles	331635	320845	36817
Particles in final map	229646	132610	22830
Resolution Relion	2.8 Å*	2.8 Å*	3.6 Å
Resolution CryoSparc	n/a	2.5Å*	3.0 Å

Models and Maps

MolProbity score	1.61	1.58	1.43
Clash score	4.79	4.47	6.2
Ramachandran Favored	94.7%	94.9%	97.6%
Ramachandran Allowed	5.3 %	5.1%	2.4%
Ramachandran Outliers	0 %	0%	0%
Rotamer outliers	0%	0%	0%
d FSC model (0/0.143/0.5)	2.5Å/2.6Å/2.9Å	2.1 Å /2.2 Å /2.7 Å	2.6Å/2.7Å/3.2Å
Accession Codes	PDB: 8PWO EMD-17996	PDB: 8PX6 EMD-18001	PDB: 8PX3 EMD-18000

Supplementary Table 4.

Cryo-EM data.

Summary of Cryo-EM data acquisition and image processing of the HBc CLPs with bound geraniol, P1dC and SLLGRM-dimers.

A1.1. SLLGRL-PEGlinker-Dimer

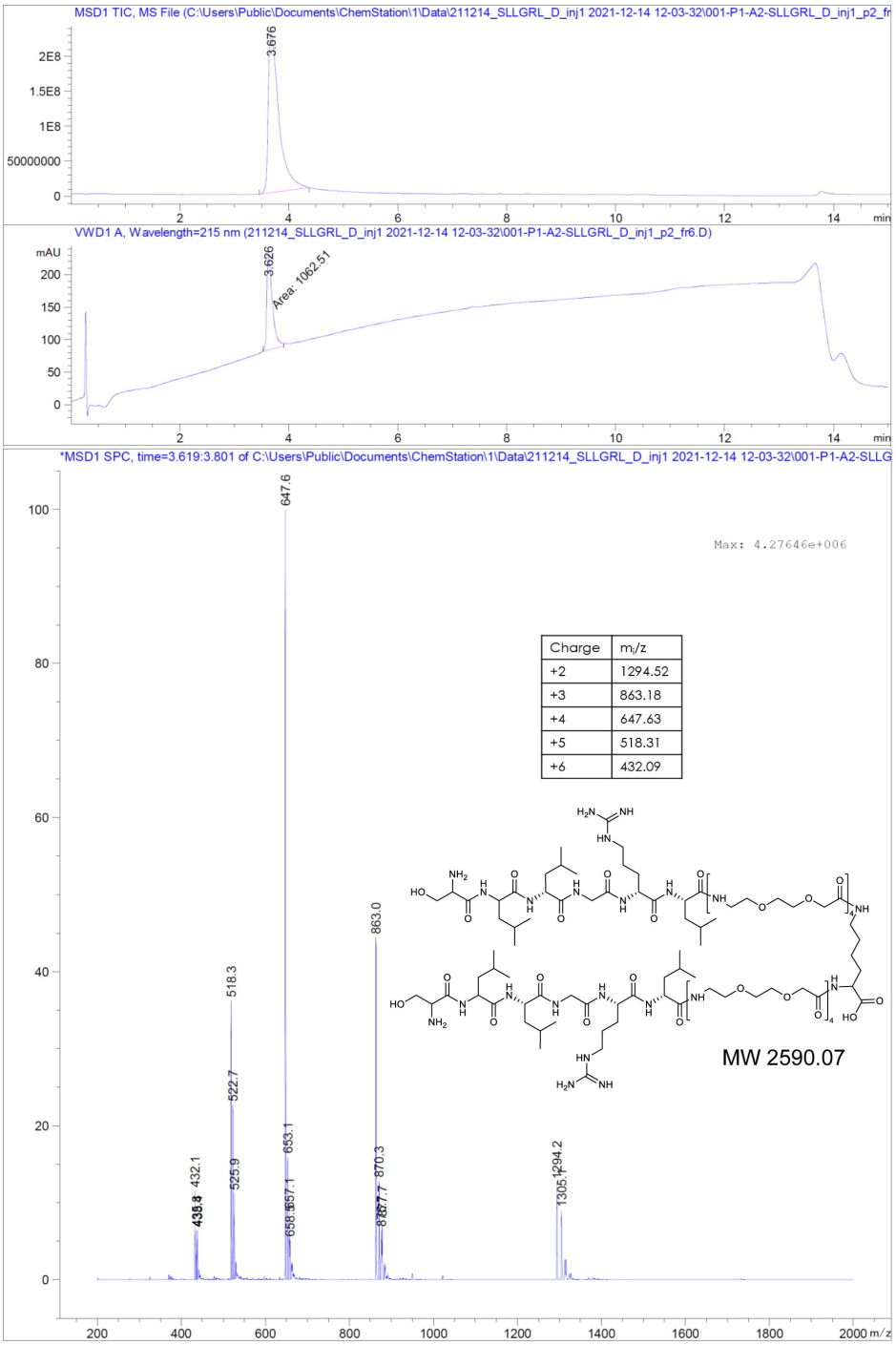

A1.2. SLLGRM-PEGlinker-Dimer (SLLGRM dimer)

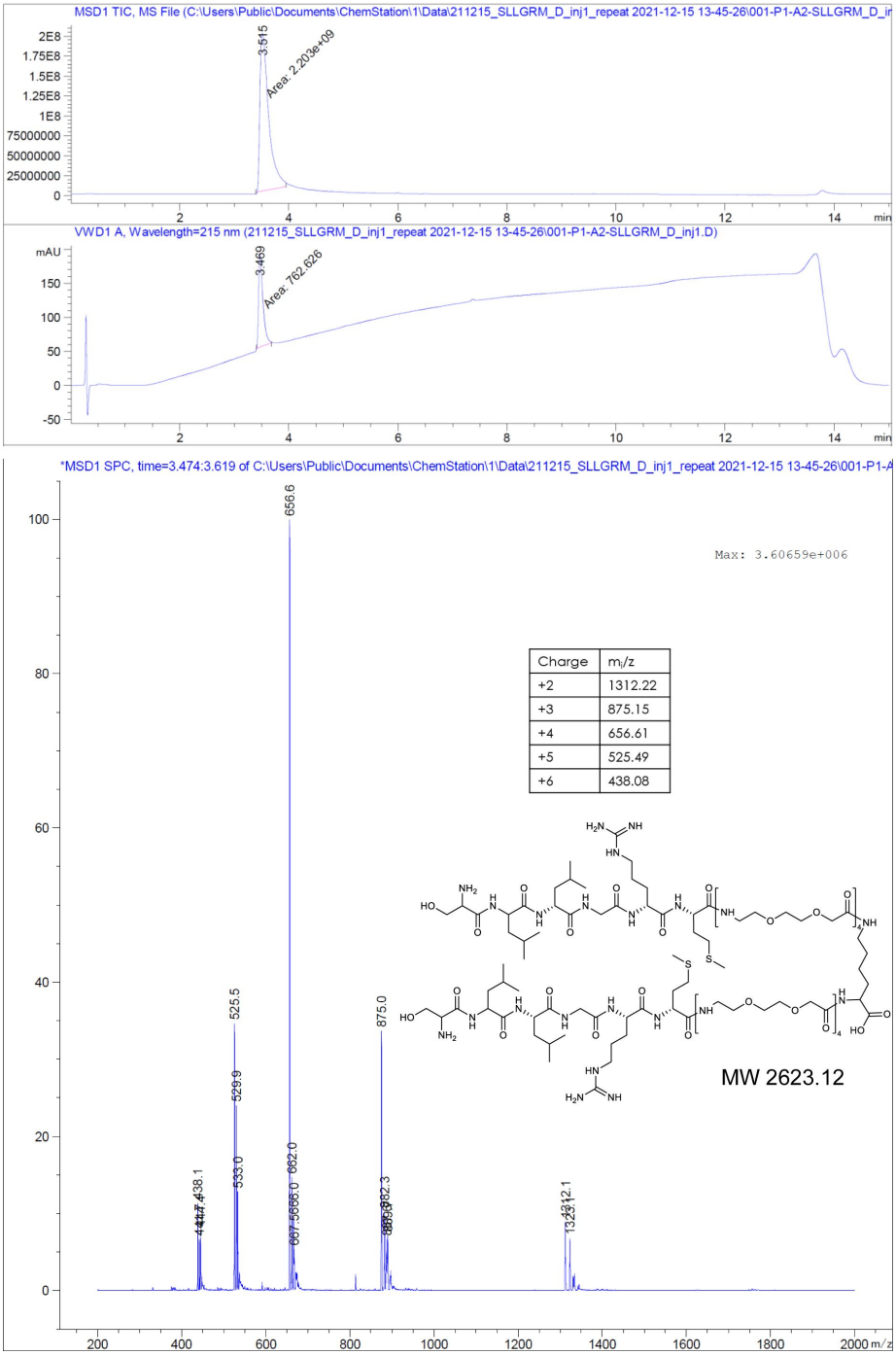

A1.3. GSLLGRMKGA-PEGlinker-Dimer (P2 dimer)

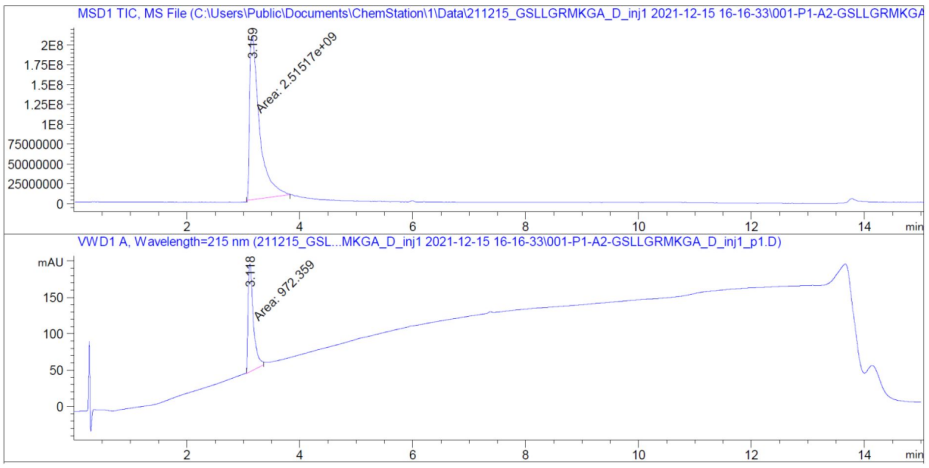

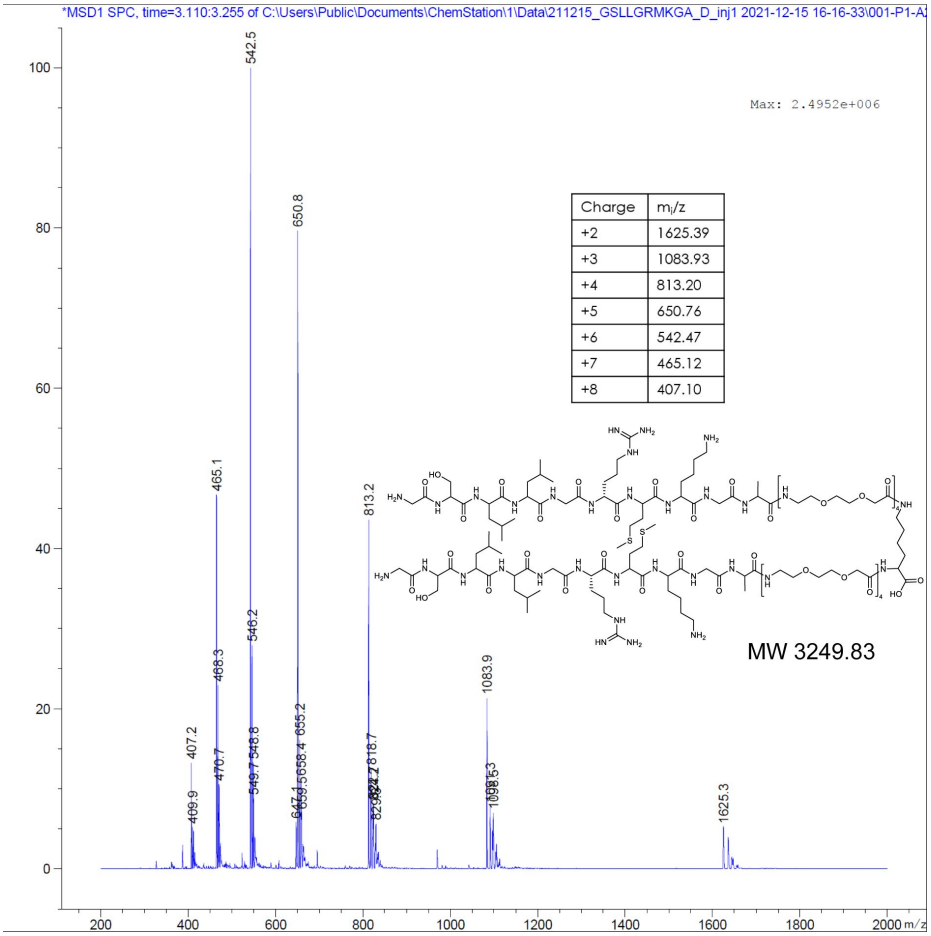

Charge	m/z
+2	1625.39
+3	1083.93
+4	813.20
+5	650.76
+6	542.47
+7	465.12
+8	407.10

MW 3249.83

A1.4 MHRSLLGRMKGA-PEGlinker-Dimer (P1 dimer)

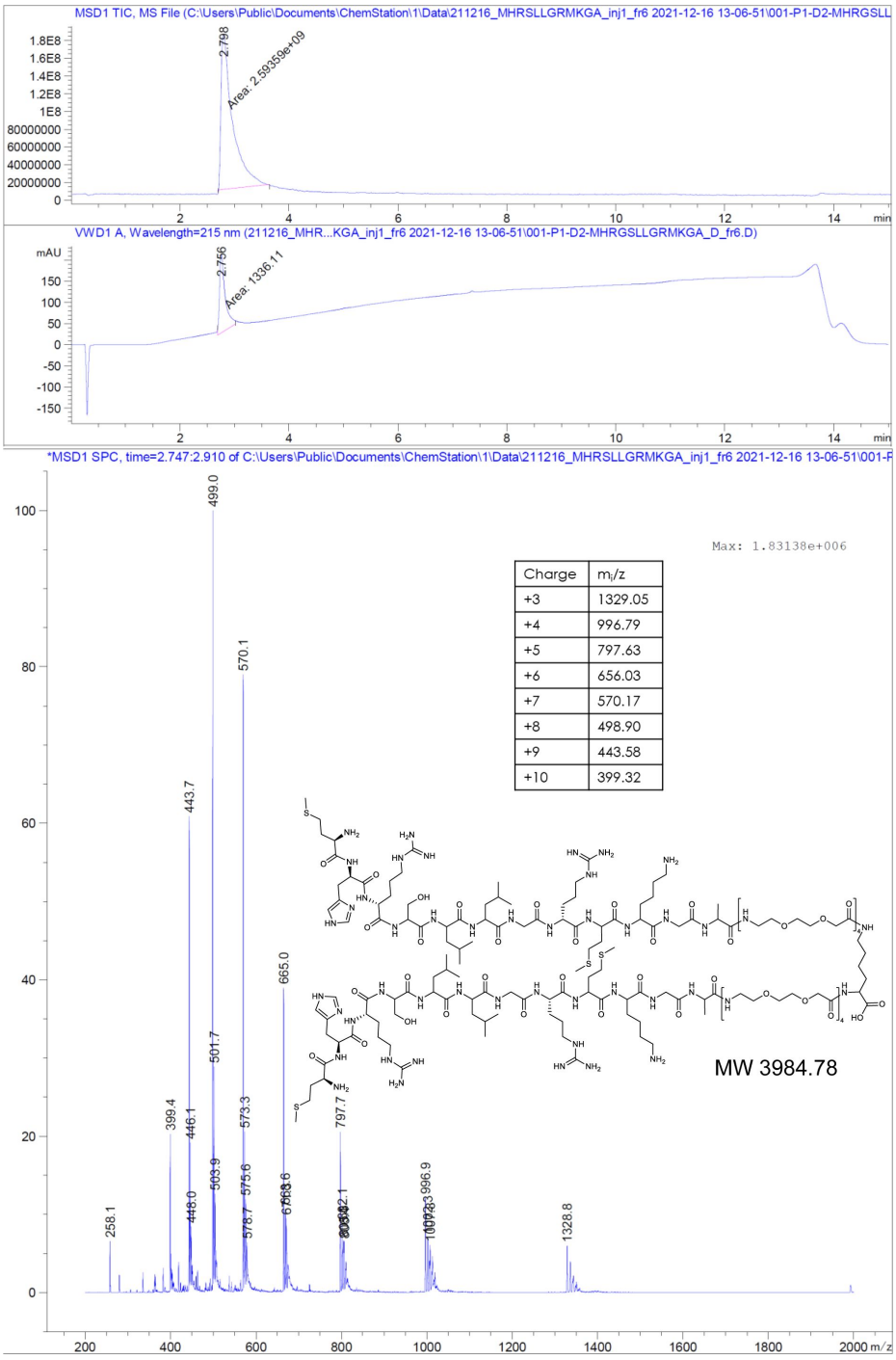

Charge	m_i/z
+3	1329.05
+4	996.79
+5	797.63
+6	656.03
+7	570.17
+8	498.90
+9	443.58
+10	399.32

A1.5. (Geranyl)$_2$-Lys2

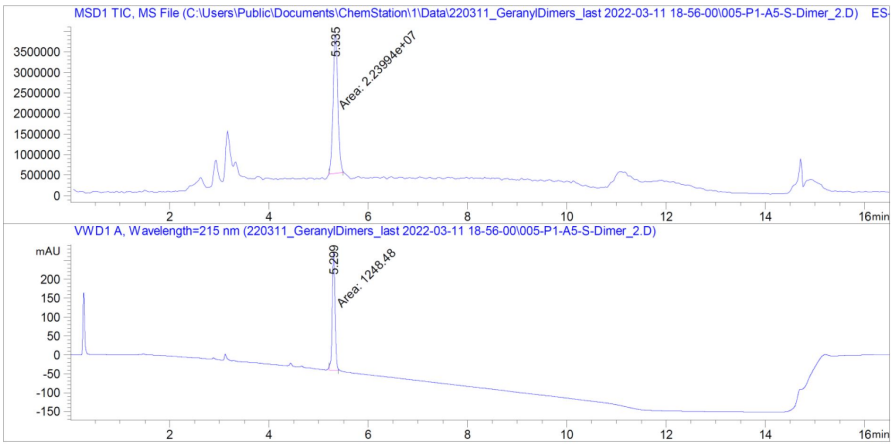

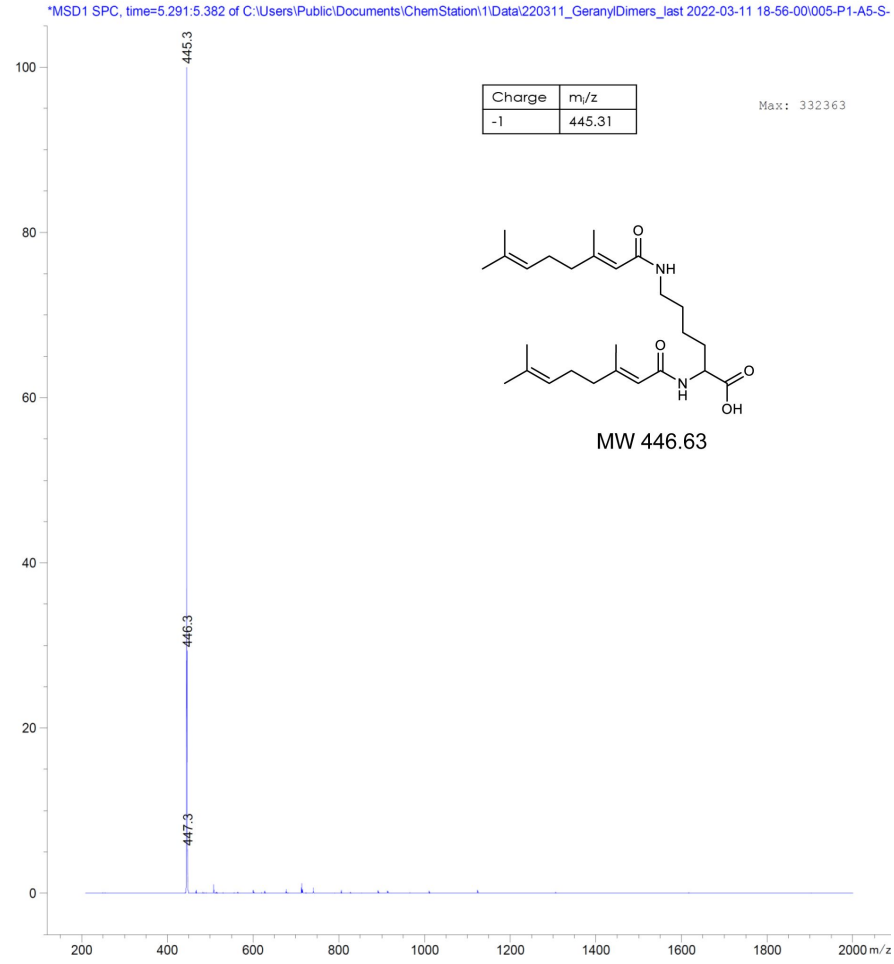

A1.6. (Geranyl-PEG3)$_2$-Lys

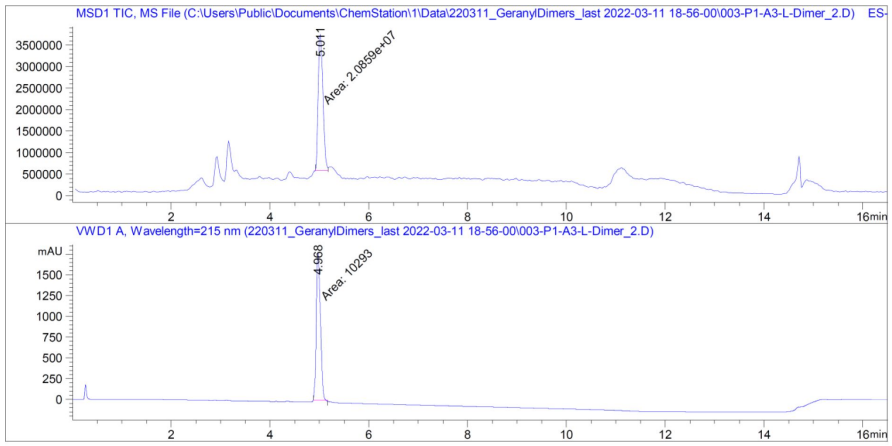

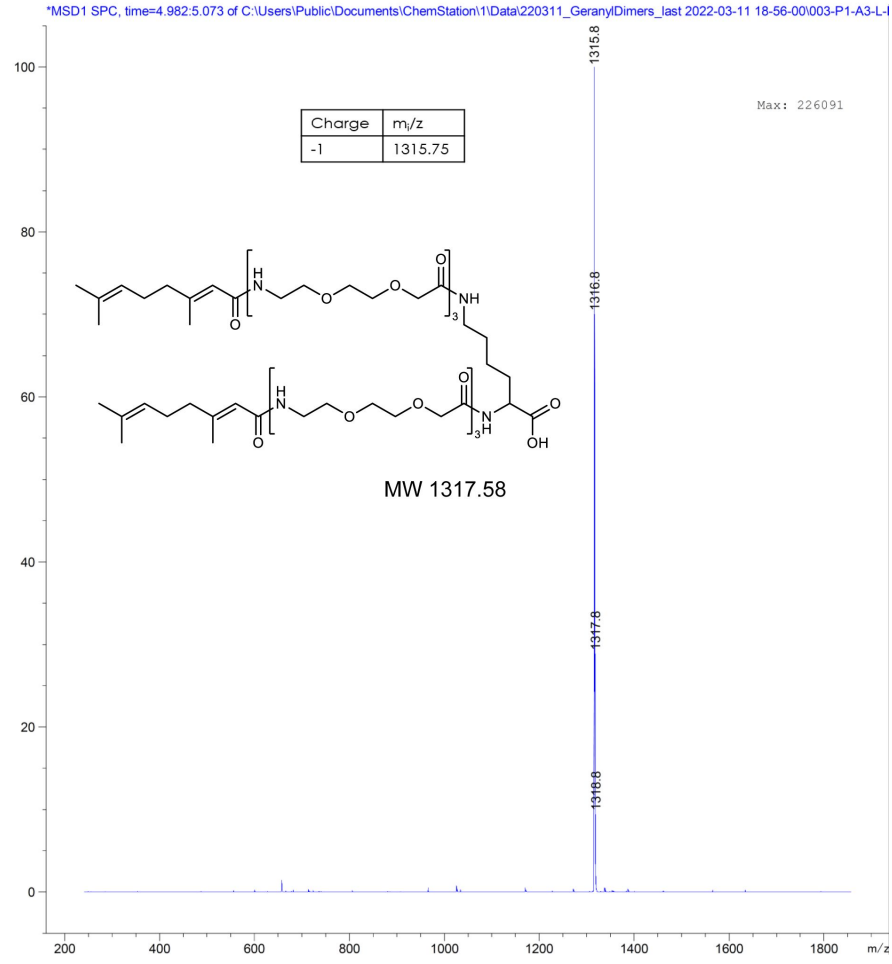

A1.7. MHRSLLGRMKGA-PEGlinker-Dimer-C (P1dC)

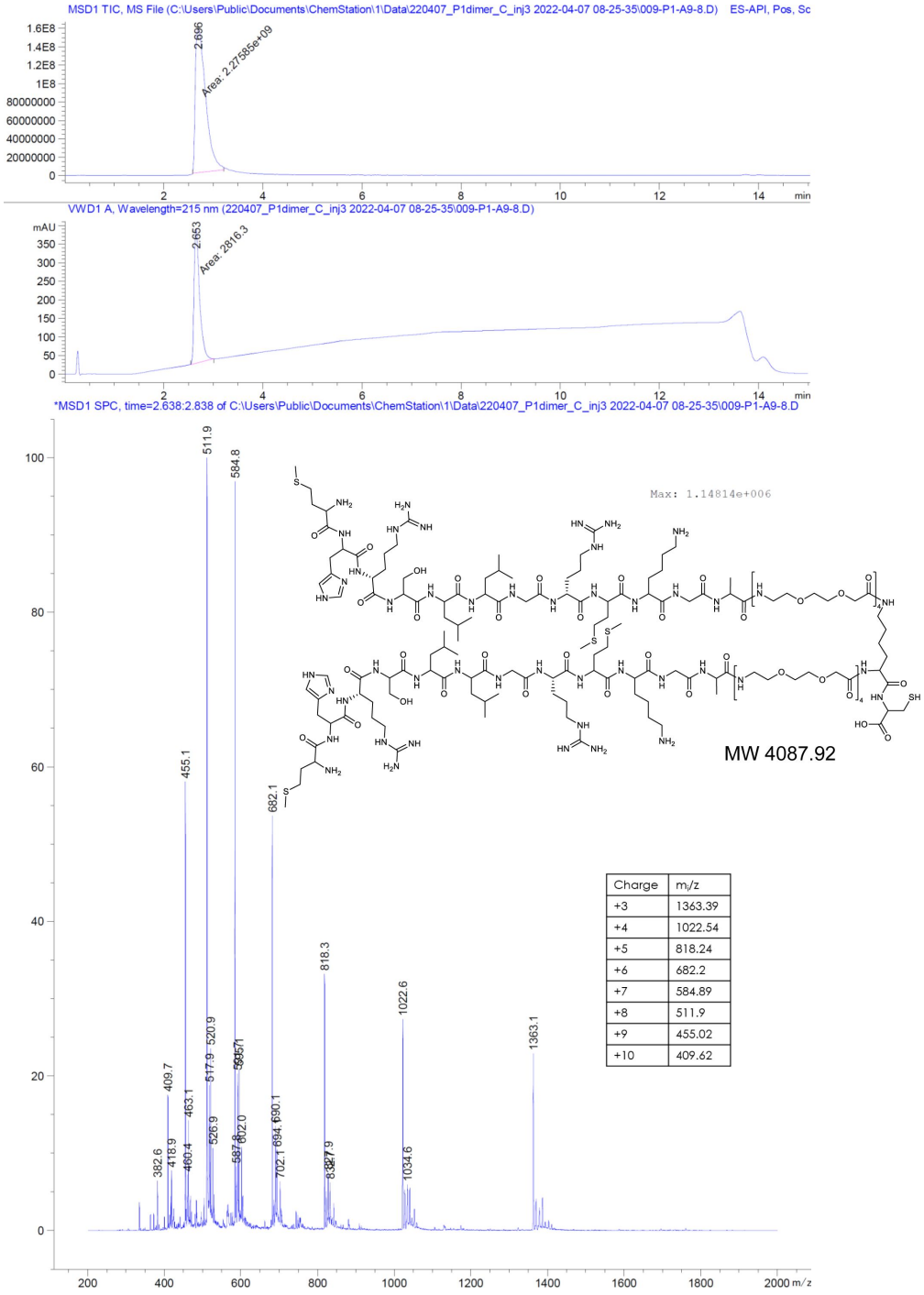

A1.8. RLHLRKAMGSMG-PEGlinker-Dimer-C (scrP1dC)

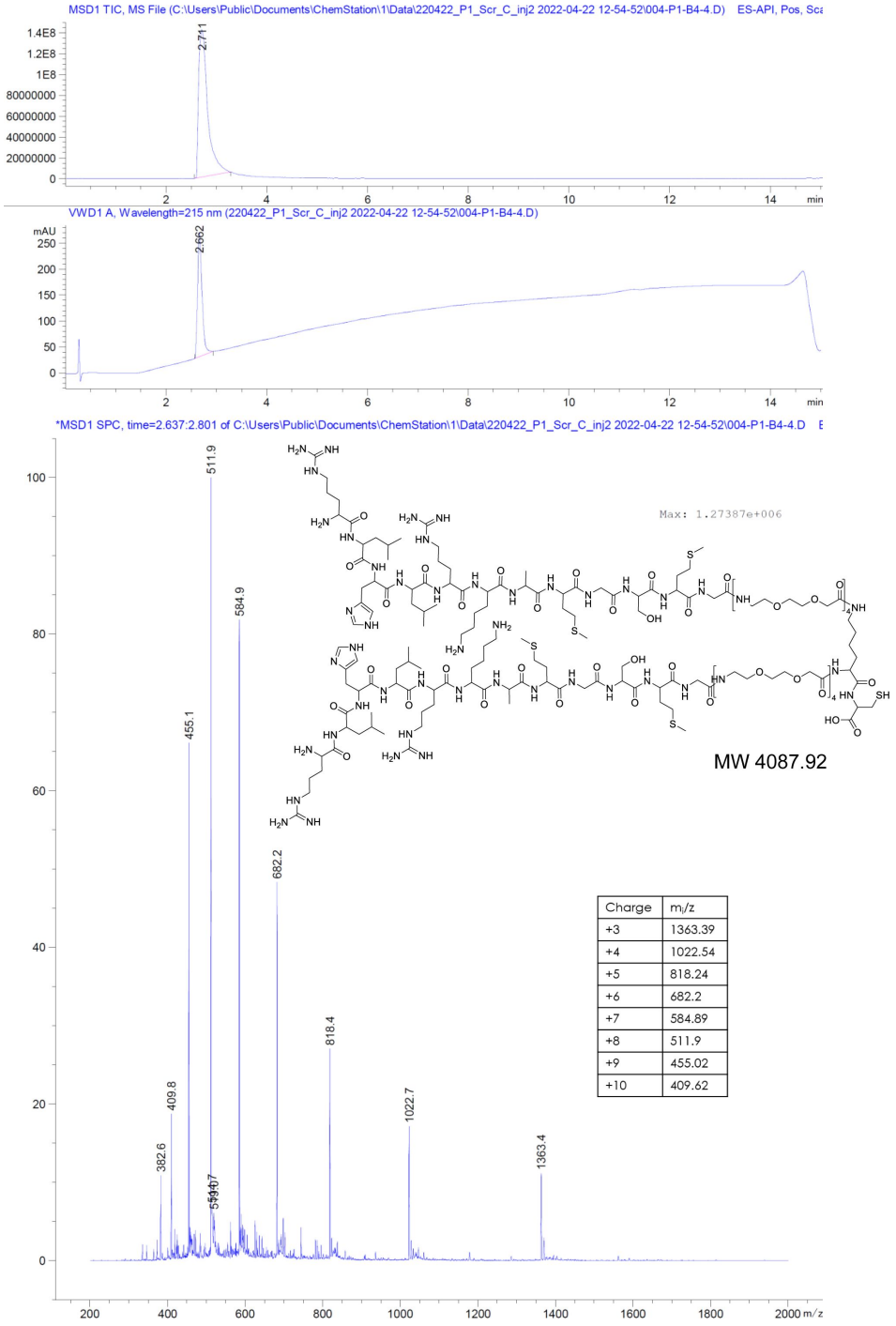

Charge	m/z
+3	1363.39
+4	1022.54
+5	818.24
+6	682.2
+7	584.89
+8	511.9
+9	455.02
+10	409.62

A1.9. TNB-C-10R

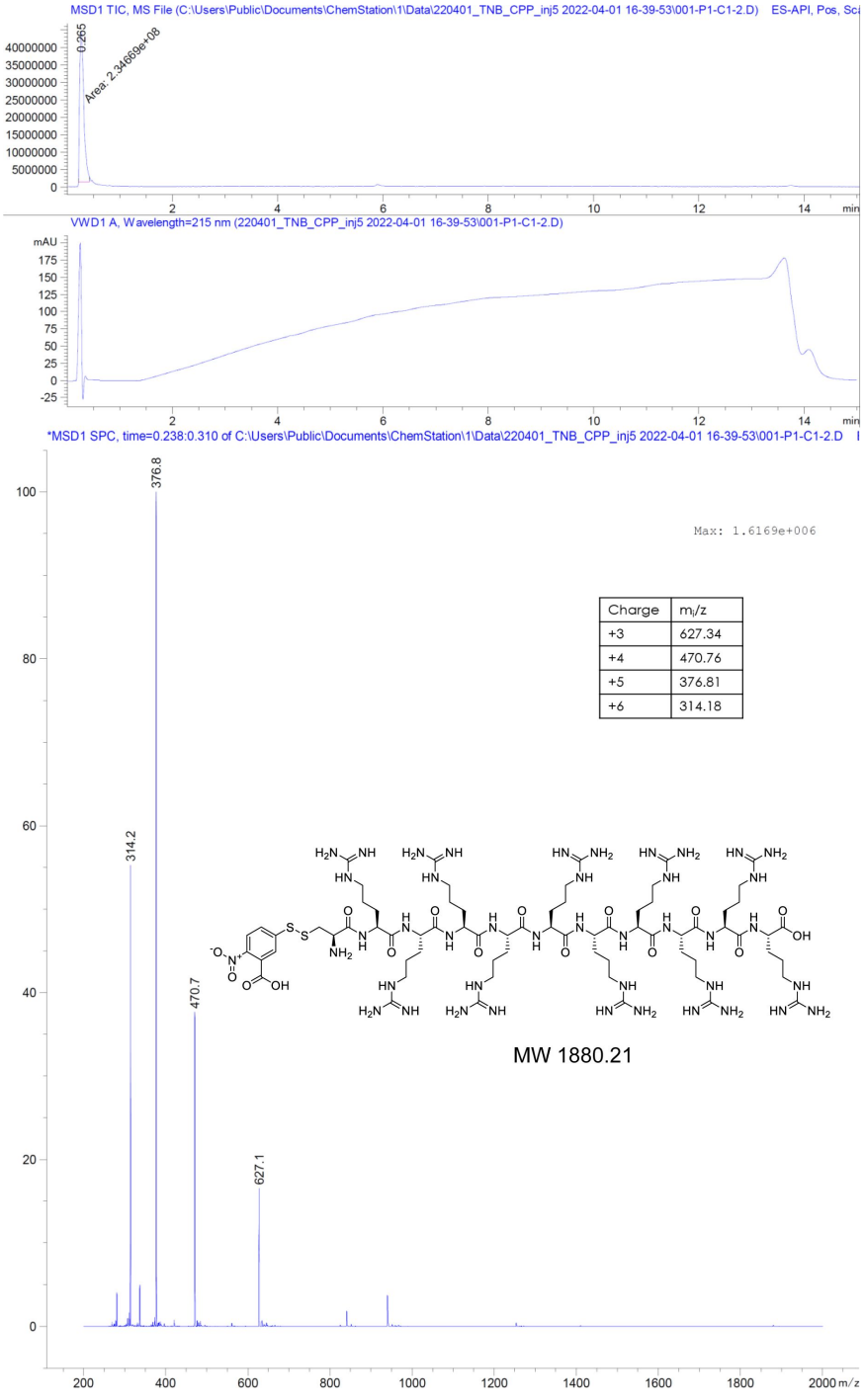
MSD1 TIC, MS File (C:\Users\Public\Documents\ChemStation\1\Data\220401_TNB_CPP_inj5 2022-04-01 16-39-53\001-P1-C1-2.D) ES-API, Pos, Sc
0.265
Area: 2.34669e+08
VWD1 A, Wavelength=215 nm (220401_TNB_CPP_inj5 2022-04-01 16-39-53\001-P1-C1-2.D)
mAU
*MSD1 SPC, time=0.238:0.310 of C:\Users\Public\Documents\ChemStation\1\Data\220401_TNB_CPP_inj5 2022-04-01 16-39-53\001-P1-C1-2.D
Max: 1.6169e+006
376.8
314.2
470.7
627.1
m/z
Charge | m/z
+3 | 627.34
+4 | 470.76
+5 | 376.81
+6 | 314.18
MW 1880.21

References

[1] Thomas D. L. (2019) **New England Journal of Medicine 380**:2041–2050

[2] Block T. M., Chang K.-M., Guo J.-T. (2021) **Annu Rev Virol 8**:437–458

[3] Cox A. L., El-Sayed M. H., Kao J. H., Lazarus J. V., Lemoine M., Lok A. S., Zoulim F. (2020) **Nat Rev Gastroenterol Hepatol 17**:533–542

[4] Dienstag J. L. (1982) **Ann Intern Med 96**

[5] World Health Organisation (2022) **Hepatitis B fact sheet** https://www.who.int/en/news-room/fact-sheets/detail/hepatitis-b

[6] (2023) **Hepatitis B Foundation, Drug Watch** https://www.hepb.org/treatment-and-management/drug-watch-2/

[7] Jeng W.-J., Papatheodoridis G. V, Lok A. S. F. (2023) **The Lancet 401**:1039–1052

[8] Menéndez-Arias L., Álvarez M., Pacheco B. (2014) **Curr Opin Virol 8**:1–9

[9] Liang T. J., Block T. M., McMahon B. J., Ghany M. G., Urban S., Guo J., Locarnini S., Zoulim F., Chang K., Lok A. S. (2015) **Hepatology 62**:1893–1908

[10] Cornberg M., Lok A. S., Terrault N. A., Zoulim F. (2020) **Hepatology 71**:1070–1092

[11] Yan H. *et al.* (2012) **Elife 1** https://doi.org/10.7554/eLife.00049

[12] Watashi K., Wakita T. (2015) **Cold Spring Harb Perspect Med 5**

[13] Ligat G., Verrier E. R., Nassal M., Baumert T. F. (2021) **Curr Opin Virol 49**:41–51

[14] Bonn B., Strängberg E., Uzelac I., Kirstgen M., Goldmann N., Glebe D., Geyer J., Lindström E. (2022) **Gut 71**:A42–A42

[15] Vaillant A. (2022) **Mol Ther Nucleic Acids 28**:168–174

[16] Vaillant A. (2019) **ACS Infect Dis 5**:675–687

[17] Gareri C., Polimeni A., Giordano S., Tammè L., Curcio A., Indolfi C. (2022) **J Clin Med 11**

[18] Yuen M.-F. *et al.* (2022) **New England Journal of Medicine 387**:1957–1968

[19] Gane E. *et al.* (2023) **J Hepatol** https://doi.org/10.1016/j.jhep.2023.05.023

[20] Bassit Leda S. R. F. (2021) **Antiviral Drug Discovery and Development** Singapore: Springer Singapore :115–138

[21] Gorsuch C. L. *et al.* (2022) **Molecular Therapy 30**:2909–2922

[22] Kim H., Ko C., Lee J.-Y., Kim M. (2021) **Molecules 26**

[23] Zheng Y., Yang L., Yu L., Zhu Y., Wu Y., Zhang Z., Xia T., Deng Q. (2023) **Viruses 15**

[24] Feld J. J. *et al.* (2022) **Antivir Ther 27**

[25] Crowther R., Kiselev N., Böttcher B., Berriman J., Borisova G., Ose V., Pumpens P. (1994) **Cell 77**:943–950

[26] Venkatakrishnan B., Katen S. P., Francis S., Chirapu S., Finn M. G., Zlotnick A. (2016) **J Virol 90**:3994–4004

[27] Stray S. J., Bourne C. R., Punna S., Lewis W. G., Finn M. G., Zlotnick A. (2005) **Proceedings of the National Academy of Sciences 102**:8138–8143

[28] Zoulim F. *et al.* (2022) **Nat Rev Gastroenterol Hepatol 19**:748–750

[29] Schlicksup C. J., Zlotnick A. (2020) **Curr Opin Virol 45**:43–50

[30] Lecoq L. *et al.* (2021) **Proceedings of the National Academy of Sciences 118** https://doi.org/10.1073/pnas.2022464118

[31] Makbul C. *et al.* (2021) **Viruses 13**

[32] Böttcher B., Tsuji N., Takahashi H., Dyson M. R., Zhao S., Crowther R. A., Murray K. (1998) **EMBO J 17**:6839–6845

[33] Makbul C., Khayenko V., Maric H. M., Böttcher B. (2021) **Microorganisms 9**

[34] Gripon P., Le Seyec J., Rumin S., Gugen-Guillouzo C. (1995) **Virology 213**:292–299

[35] Koh C. *et al.* (2015) **Lancet Infect Dis 15**:1167–1174

[36] Roseman A. M., Berriman J. A., Wynne S. A., Butler P. J. G., Crowther R. A. (2005) **Proceedings of the National Academy of Sciences 102**:15821–15826

[37] Böttcher B., Nassal M. (2018) **J Mol Biol 430**:4941–4954

[38] Rost M., Mann S., Lambert C., Döring T., Thomé N., Prange R. (2006) **Journal of Biological Chemistry 281**:29297–29308

[39] Le Pogam S., Yuan T. T.-T., Sahu G. K., Chatterjee S., Shih C. (2000) **J Virol 74**:9099–9105

[40] Yuan T. T.-T., Shih C. (2000) **J Virol 74**:4929–4932

[41] Yuan T. T.-T., Sahu G. K., Whitehead W. E., Greenberg R., Shih C. (1999) **J Virol 73**:5731–5740

[42] Ehata T., Omata M., Yokosuka O., Hosoda K., Ohto M. (1992) **Journal of Clinical Investigation 89**:332–338

[43] Dyson M. R., Murray K. (1995) **Proceedings of the National Academy of Sciences 92**:2194–2198

[44] Wynne S. A., Crowther R. A., Leslie A. G. W. (1999) **Mol Cell 3**:771–780

[45] Zhao R., So M., Maat H., Ray N. J., Arisaka F., Goto Y., Carver J. A., Hall D. (2016) **Biophys Rev 8**:445–471

[46] Schneider A. F. L., Benz L. S., Lehmann M., Hackenberger C. P. R. (2021) **Angewandte Chemie International Edition 60**:22075–22080

[47] Schneider A. F. L., Kithil M., Cardoso M. C., Lehmann M., Hackenberger C. P. R. (2021) **Nat Chem 13**:530–539

[48] Hadden J. A., Perilla J. R., Schlicksup C. J., Venkatakrishnan B., Zlotnick A., Schulten K. (2018) **Elife 7** https://doi.org/10.7554/eLife.32478

[49] Forsberg B. O., Shah P. N. M., Burt A. (2023) **Nat Commun 14**

[50] Briday M. *et al.* (2022) **Chem Sci 13**:8840–8847

[51] Yuan T. T.-T., Sahu G. K., Whitehead W. E., Greenberg R., Shih C. (1999) **J Virol 73**:5731–5740

[52] Bruss V. (2007) **World J Gastroenterol 13**

[53] Ponsel D., Bruss V. (2003) **J Virol 77**:416–422

[54] Koschel M., Thomssen R., Bruss V. (1999) **J Virol 73**:2153–2160

[55] Wu G. *et al.* (2013) **Antimicrob Agents Chemother 57**:5344–5354

[56] Pavlova A., Korablyov M., Chipot C., Gumbart J. (2018) **Biophys J 114**

[57] Perilla J. R., Hadden J. A., Goh B. C., Mayne C. G., Schulten K. (2016) **J Phys Chem Lett 7**:1836–1844

[58] Pavlova A., Bassit L., Cox B. D., Korablyov M., Chipot C., Patel D., Lynch D. L., Amblard F., Schinazi R. F., Gumbart J. C. (2022) **J Med Chem 65**:4854–4864

[59] Punjani A., Zhang H., Fleet D. J. (2020) **Nat Methods 17**:1214–1221

[60] Casañal A., Lohkamp B., Emsley P. (2020) **Protein Science 29**:1055–1064

[61] Liebschner D. *et al.* (2019) **Acta Crystallogr D Struct Biol 75**:861–877

[62] Prisant M. G., Williams C. J., Chen V. B., Richardson J. S., Richardson D. C. (2020) **Protein Science 29**:315–329

[63] Yang Z., Lasker K., Schneidman-Duhovny D., Webb B., Huang C. C., Pettersen E. F., Goddard T. D., Meng E. C., Sali A., Ferrin T. E. (2012) **J Struct Biol 179**:269–278

[64] Galibert F., Mandart E., Fitoussi F., Tiollais P., Charnay P. (1979) **Nature 281**:646–650

[65] (2011) **D. G. Gibson, 2011, pp. 349–361.** :349–361

[66] Dikmans A., Beutling U., Schmeisser E., Thiele S., Frank R. (2006) **QSAR Comb Sci 25**:1069–1080

[67] Schindelin J. *et al.* (2012) **Nat Methods 9**:676–682

[68] Pettersen E. F., Goddard T. D., Huang C. C., Couch G. S., Greenblatt D. M., Meng E. C., Ferrin T. E. (2004) **J Comput Chem 25**:1605–1612

Author information

Vladimir Khayenko[+]
Rudolf Virchow Center, Center for Integrative and Translational Bioimaging; University of Würzburg, Würzburg Germany, Biocenter, University of Würzburg, Würzburg, Germany

[+]equal contribution

Cihan Makbul[+]
Rudolf Virchow Center, Center for Integrative and Translational Bioimaging; University of Würzburg, Würzburg Germany, Biocenter, University of Würzburg, Würzburg, Germany

[+]equal contribution

Clemens Schulte
Rudolf Virchow Center, Center for Integrative and Translational Bioimaging; University of Würzburg, Würzburg Germany, Biocenter, University of Würzburg, Würzburg, Germany

Naomi Hemmelmann
Rudolf Virchow Center, Center for Integrative and Translational Bioimaging; University of Würzburg, Würzburg Germany, Biocenter, University of Würzburg, Würzburg, Germany

Sonja Kachler
Rudolf Virchow Center, Center for Integrative and Translational Bioimaging; University of Würzburg, Würzburg Germany, Biocenter, University of Würzburg, Würzburg, Germany

Bettina Böttcher
Rudolf Virchow Center, Center for Integrative and Translational Bioimaging; University of Würzburg, Würzburg Germany, Biocenter, University of Würzburg, Würzburg, Germany
ORCID iD: 0000-0002-7962-4849

For correspondence: bettina.boettcher@uni-wuerzburg.de

Hans M Maric
Rudolf Virchow Center, Center for Integrative and Translational Bioimaging; University of Würzburg, Würzburg Germany, Biocenter, University of Würzburg, Würzburg, Germany
ORCID iD: 0000-0002-2719-4752

For correspondence: hans.maric@uni-wuerzburg.de

Editors

Reviewing Editor
Mauricio Comas-Garcia
Universidad Autónoma de San Luis Potosí, San Luis Potos, Mexico

Senior Editor
Volker Dötsch
Goethe University Frankfurt, Frankfurt am Main, Germany

Reviewer #1 (Public review):

Summary:

In this paper, the authors present an interesting strategy to interfere with the HBV life cycle: the preparation of geranyl and peptides' dimers that could impede the correct assembly of hepatitis B core protein HBc into viable capsids. These dimers are of different nature, depending on the HBc site the authors plan to target. A preliminary study with geranyl dimers (targeting a hydrophobic site of HBc) was first investigated. The second series deals with peptide-PEG linker-peptide dimers, targeting the tips of HBc dimer spikes.

Strengths:

This work is very well conducted, combining ITC experiments (for determination of dimers' KD), cellular effects (thanks to the grafting of previously developed dimers with polyarginine-based cell penetrating peptide) HBV infected HEK293 cells and Cryo-EM studies.
The findings of these research teams unambiguously demonstrated the interest of such dimeric structures in impeding the correct HBV life cycle and thus, could bring solutions in the control of its development. Ultimately, a new class of HBV Capside Assembly Modulators could arise from this study.
There is no doubt that this work could bring very interesting information for people working on VHB.

Comments on revisions:

Minor corrections have been made in this revised version of this work, according to the remarks of the reviewers.

https://doi.org/10.7554/eLife.98827.2.sa2

Reviewer #2 (Public review):

Summary:

Vladimir Khayenko et al. discovered two novel binding pockets on HBc with in vitro binding and electron microscopy experiments. While the geranyl dimer targeting a central hydrophobic pocket displayed a micromolar affinity, the P1-dimer binding to the spike tip of HBc has a nanomolar affinity. In the turbidity assay and at the cellular level, an HBc aggregation from peptide crosslinking was demonstrated.

Strengths:

The study identifies two previously unexplored binding pockets on HBc capsids and develops novel binders targeting these sites with promising affinities.

Weaknesses:

While the in vitro and cellular HBc aggregation effects are demonstrated, the antiviral potential against HBV infection is not directly evaluated in this study.

https://doi.org/10.7554/eLife.98827.2.sa1

Author response:

The following is the authors' response to the original reviews.

We appreciate the positive assessment and agree that the experimental data offer valuable insights into HBV capsid assembly inhibition. Based on the reviewers' suggestions, we have clarified the cryo-EM data and added structural and mechanistic details throughout the manuscript, which we believe significantly enhance its overall clarity and impact. The manuscript now better reflects a promising strategy to interfere with the HBV life cycle. We have carefully addressed all comments to improve both the clarity and quality of the manuscript.

Response to Public Reviews

We greatly appreciate the insightful comments and suggestions from the reviewers. Below, we provide responses to the points raised in the public reviews.

> ***Reviewer #1 (Public Review):***
>
> *Summary:*
>
> *In this paper, the authors present an interesting strategy to interfere with the HBV life cycle: the preparation of geranyl and peptides' dimers that could impede the correct assembly of hepatitis B core protein HBc into viable capsids. These dimers are of different nature, depending on the HBc site the authors plan to target. A preliminary study with geranyl dimers (targeting a hydrophobic site of HBc) was first investigated. The second series deals with peptide-PEG linker-peptide dimers, targeting the tips of HBc dimer spikes.*
>
> *Strengths:*
>
> *This work is very well conducted, combining ITC experiments (for determination of dimers' KD), cellular effects (thanks to the grafting of previously developed dimers with polyarginine-based cell penetrating peptide) HBV infected HEK293 cells and Cryo-EM studies.*
>
> *The findings of these research teams unambiguously demonstrated the interest of such dimeric structures in impeding the correct HBV life cycle and thus, could bring solutions in the control of its development. Ultimately, a new class of HBV Capside Assembly Modulators could arise from this study.*
>
> *There is no doubt that this work could bring very interesting information for people working on VHB.*
>
> *Weaknesses:*
>
> *Some minor corrections must be made, especially for a more precise description of the strategy and the chemical structure of the designed new VHB capsid assembly modulators.*

We are grateful for the positive feedback on the experimental design, the combination of ITC, cellular effects, and Cryo-EM studies, and the potential for developing new classes of HBV Capsid Assembly Modulators (CAMs). In the revised version we have clarified the design rationale for the choice of the PEG linker length in the Supplementary Information, linking it to the structural measurements of the capsid. Chemical structures and detailed molecular formulas were added and terms have been corrected. A scrambled dimeric peptide served as a negative control, which showed no binding, confirming the specificity of our designed peptide and ruling out non-specific interactions from other elements of the molecules such as the linkers. Finally, we have revised the nomenclature for the geranyl dimers to better reflect the chemical structure. All figures, including Figure 3, have been updated to high-resolution. All mentioned typos have been corrected. Consultation dates have been added to the website references. HPLC terminology was corrected.

> ***Reviewer #2 (Public Review):***
>
> *Summary:*
>
> *Vladimir Khayenko et al. discovered two novel binding pockets on HBc with in vitro binding and electron microscopy experiments. While the geranyl dimer targeting a central hydrophobic pocket displayed a micromolar affinity, the P1-dimer binding to the spike tip of HBc has a nanomolar affinity. In the turbidity assay and at the cellular level, an HBc aggregation from peptide crosslinking was demonstrated.*
>
> *Strengths:*
>
> *The study identifies two previously unexplored binding pockets on HBc capsids and develops novel binders targeting these sites with promising affinities.*
>
> *Weaknesses:*
>
> *While the in vitro and cellular HBc aggregation effects are demonstrated, the antiviral potential against HBV infection is not directly evaluated in this study.*

Thank you for recognizing the innovative approach of our work and the potential for developing novel antivirals targeting HBc. We have now included additional discussion on potential future experiments aimed at evaluating the compounds' effects on cellular physiology and viral infectivity.

> ***Reviewer #3 (public Review):***
>
> *Summary:*
>
> *HBV is a continuing public health problem and new therapeutics would be of great value. Khayenko et al examine two sites in the HBc dimer as possible targets for new therapeutics. Older drugs that target HBc bind at a pocket between two HBc dimers. In this study Khayenko et al examine sites located in the four helix bundle at the dimer interface.*
>
> *The first site is a pocket first identified as a triton100 binding site. The authors suggest it might bind terpenes and use geraniol as an example. They also test a decyl maltose detergent and a geraniol dimer intended for bivalent binding. The KDs were all in the 100μM range. Cryo-EM shows that geraniol binds the targeted site.*
>
> *The second site is at the tip of the spike. Peptides based on a 1995 study (reference 43) were investigated. The authors test a core peptide, two longer peptides, and a dimer of the longest peptide. A deep scan of the longest monomer sequence shows the*

> *importance of a core amino acid sequence. The dimeric peptide (P1-dimer) binds almost 100 fold better than the monomer parent (P1). Cryo-EM structures confirm the binding site. The dimeric peptide caused HBc capsid aggregation When HBc expressing cells were treated with active peptide attached to a cell penetrating peptide, the peptide caused aggregation of HBc antigen mirroring experiments with purified proteins.*
>
> *Strengths:*
>
> *The two sites have not been well investigated. This paper marks a start. The small collection of substrates investigated led to discovery of a dimeric peptide that leads to capsid aggregation, presumably by non-covalent crosslinking. The structures determined could be very useful for future investigations.*
>
> *Weaknesses:*
>
> *In this draft, the rational for targets for the triton x100 site is not well laid out. The target molecules bind with KDs weaker that 50μM. The way the structural results are displayed, one cannot be sure of the important features of binding site with respect to the the substrate. The peptide site and substrates are better developed, but structural and mechanistic details need to be described in greater detail.*

We appreciate the reviewer's positive comments on identifying and targeting previously unexplored sites on HBc, and the potential utility of our dimeric peptides in future studies. We have revised the Results section to better explain the rationale behind targeting the hydrophobic binding site. Additionally, the structures have been revised for clearer presentation, and we now emphasize the key features of the binding site and the role of substrate specificity.

> ***Recommendations For The Authors:***
>
> ***Reviewer #1 (Recommendations For The Authors):***
>
> *For clarity, the chemical structure of SLLGRM peptide, geraniol and HAP molecules must be indicated, preferably in Fig. 1 (at least in the Supplementary Information section).*

We have now included the chemical structures of the SLLGRM peptide, geraniol, and HAP molecules for clarity in Figure 1 and in the main manuscript to ensure they are easily accessible for reference and to provide further detail and context.

> *In the same idea, in Fig. 1 (and in the text): The molecular formula of heteroaryldihydropyrimidine HAP must be clearly indicated, as the nature of the heteroatom (S, O, N?) in this "heteroaryl" derivative is not indicated.*

The full molecular formula of HAP (((2S)-1-[[(4R)-4-(2-chloranyl-4-fluoranyl-phenyl)-5-methoxycarbonyl-2-(1,3-thiazol-2-yl)-1,4-dihydropyrimidin-6-yl]methyl]-4,4-bis(fluoranyl)-pyrrolidine-2-carboxylic acid), is now included the figure legend.

> *with a polyethylene glycol (PEG) linker that could bridge the distance of 38 Å between the two opposing hydrophobic pockets": what is the rationale of the design of this linker? Authors must explain briefly why/how they have chosen this linker length and nature (please indicate a reference for the appropriate choice of PEG linker). Same remarks for dimers targeting the capsid spike tips, having 50 angstroms PEG linkers. So, the choice of the linker length must be clearly explained and not be only mentioned in the sentence of the discussion part "Using our structural knowledge of the capsid, particularly the distances between the spikes.*

We have now better clarified the rationale for the design of the PEG linker length. The linker lengths were specifically chosen based on structural knowledge of the capsid, particularly the measured distances between the spike tips (60 Å) and the hydrophobic pockets (40 Å). In the Supplementary Information (Supplementary Figure 1), we now clearly explain how these measurements guided the choice of PEG linker length, allowing for optimal bridging and interaction between the binding sites. This supplementary figure now explicitly connects the design rationale to the specific structural features of the capsid.

> *I do not agree with the authors when they claim a "nanomolar affinity of 312 nM". To me, a nanomolar affinity would require several of few tens of nanoM (but not three hundreds) ... So, please correct with "sub-micromolar affinity of 312 nM" and all the other parts of the manuscript (title and caption of Figure 3..., "the peptide dimer (P1dC) with nanomolar affinity" "nanomolar levels"...).*

We thank the Rev#1 for pointing this out. Since the term "nanomolar affinity" can indeed be interpreted as referring to the lower end of the nanomolar range, rather than values close to 300 nM we have revised the manuscript to refer to the "sub-micromolar affinity" where applicable. This change has been made throughout the manuscript, including the subtitles and figure captions, and the text.

> *The drug design strategy was to combine two peptides showing low affinity, attached by a PEG linker with an appropriate length and appears obvious to me. But a control experiment is anyway missing: the peptide-PEG linker derivative (not the dimer peptide-PEG linker-peptide...) should have been evaluated for an unambiguous proof of concept of these dimeric peptides. To my opinion, for the publication of this work, these experiments should be brought (eg, when describing the affinities of SLLGR dimers). I agree that Cryo-EM experiments bring evidences of the dimer binding but the affinity values for (peptide-PEG linker) derivatives would bring an additional proof (as the PEG flexible linkers was not resolved by Cryo-EM).*

Thank you for your thoughtful comment regarding the use of a monovalent control for the peptide-PEG linker. A scrambled dimeric peptide serves as a negative control. In ITC it showed no binding at all. Thereby ruling out possibly unspecific interactions mediated by the introduced PEG linker or handle itself.

Given the complete lack of binding with the scrambled dimeric peptide, we believe this thoroughly excludes the need for an additional monovalent control, as it provides strong evidence that the observed binding is driven specifically by the designed peptide sequence and not by the linker or other structural components. We have now made this clarification more explicit in the revised manuscript to avoid any ambiguity. We hope this addresses your concern, and we appreciate your suggestion to further strengthen the rigor of the work. Despite its identical charge, molecular weight and atom composition the scrambled control did not cause HBc aggregation in living cells, thus indicating sequence specific action of the aggregating dimer.

> *The nomenclature of the dimers must be modified because there is no logic between the name "long dimer" and the chemical structure. Particularly, the number of ethylene glycol motifs must be indicated: authors have to find an appropriate nomenclature indicating both the linker length and nature (small molecule or peptide) of the bivalent parts (and hence, do not mention anymore "short geranyl dimer" "long geranyl dimer").*

Thank you for your valuable suggestion regarding the nomenclature of the dimers. We agree that the terms "short geranyl dimer" and "long geranyl dimer" do not fully reflect the chemical structure of the molecules. In response, we have revised the nomenclature to

provide a clearer indication of both the linker length and the nature of the bivalent parts. We now refer to the dimers as $(Geranyl)_2$-Lys for the dimer with two geranyl groups attached to lysine and $(Geranyl\text{-}PEG3)_2$-Lys for the dimer with a PEG3 linker (three ethylene glycol units) between the lysine amine and the geranyl groups. These revised names more accurately describe the structural differences and should avoid any ambiguity.

> *Lines 198-199: "Among these, the dimerized P1 exhibited a higher 198 occupation of the binding site, as illustrated in Supplementary Figure 9." But in Supp. Fig. 9, dimer P1dC (10) is described. As the text above is describing P1-dimer (9), the Supp. Fig. 9 must be provided, if available. If not, please modify this conclusion accordingly. In the text, when mentioning dimerized P1 peptide, authors must indicate with which compound it deals: (9) or (10)?*

Thank you for your careful reading of the manuscript and for pointing out the discrepancy. In Supplementary Figure 9, the dimer described is P1dC, not P1d. The text has been revised to clarify this. We appreciate your attention to detail.

> *Please note that the graphic quality of Figure 3 is bad as it results in pixelized drawings (especially for the chemical structures).*

Thank you for your feedback regarding the quality of Figure 3. We have now updated all figures, including Figure 3, to high-resolution PNG format with 300-500 dpi to ensure optimal graphic quality. This should resolve the pixelization issue, particularly for the chemical structures.

> *Minor typos: "clinical studies, a third are CAMs.[6]" "to the spike base hydrophobic pocket" "geraniol affinity to the central hydrophobic pocket, we designed"*

We have corrected the punctuation in the mentioned sentences and appreciate your careful review of the manuscript.

> *Concerning the citation of a website (references 5 and 6), I guess that the consultation date should be mentioned.*

We have now updated the references accordingly, including the consultation dates.

> *In the Materials and Methods part, Peptide synthesis paragraph, authors must write "semi-preparative HPLC.*

It's now corrected to "semi-preparative HPLC".

> *In the supplementary information file, 1H and 13C NMR spectrum for the small molecule "Short Geranyl Dimer (SGD)" should be provided.*

The purity and identity of this Geranyl derivate were confirmed through UV detection in LC-MS and supported by the mass spectra, which provide robust and clear evidence of the compound's structure and well-accepted method for confirming the structure in this context. While we understand the value of NMR in structural analysis, we believe that additional analytical evidence is not critical for this study.

> ***Reviewer #2 (Recommendations For The Authors):***
>
> *Overall, this study presents an innovative approach to target the HBV core protein and paves the way for developing new classes of antivirals with a distinct mechanism of*

> *action. The findings expand the current knowledge of druggable sites on HBc capsids and provide promising lead compounds. Future studies exploring the antiviral effects and optimizing the binders for therapeutic applications would be valuable next steps.*

We sincerely thank the reviewer for the positive assessment of our work and for highlighting its innovative approach to targeting the HBV core protein. We appreciate your recognition of the study's potential in paving the way for developing new classes of antivirals with distinct mechanisms of action. Below, we provide responses to each of the points raised.

> *The significance of the central hydrophobic pocket as a target may require additional experiments for validation. Currently, the substrate binding activity is relatively low and appears to have a non-significant impact on HBc.*

We agree that the central hydrophobic pocket exhibits relatively weak binding affinity with the ligands tested in this study. However, we have provided additional structural evidence and affinity data to support its relevance as a druggable site. In recognition of the weak affinity of these small molecules, we expanded our focus to include peptide-based binders, which yielded higher affinities, particularly when dimerized.

> *It might be more effective to present Figure 1B after summarizing all the results.*

We understand the reviewer's suggestion. However, we decided to highlight and summarize the major findings early in the manuscript. We included Figure 1B at the beginning to allow readers to quickly grasp the core concepts and outcomes of our study.

> *The labels for P1/P2 are presented in Figure 1A, yet their definitions are not provided until the second part of the Results section.*

We appreciate the reviewer's observation. While see a benefit of showing three trackable sites on HBV early and as an overview but we also agree that the early presentation of P1/P2 could lead to some confusion. To resolve this, we have revised the figure to introduce only on the minimal peptide to avoid any ambiguity. The full dimer sequences and names are introduced later.

> *Further investigation of the cytotoxic potential of peptide-induced HBc aggregation is necessary.*

Investigating the cytotoxicity together with infectivity is an important future direction but outside the scope of this study. We now elaborate on this point in the discussion.

> ***Reviewer #3 (Recommendations For The Authors):***
>
> *Two sites in the dimer interface are shown to bind ligands. It is not shown that filling these regions will change infection. The exhaustive studies by Bruss showed point mutations directly alter infection and would be of value to discuss.*

We thank Rev#3 for this very helpful comment. We now highlight how point mutations in these regions were shown to affect HBV infectivity. Thereby providing a link between our findings and how ligand binding might influence the viral life cycle.

> *It is not shown whether the two sites interact. Molecular dynamics by Hadden or Gumbart may be informative. The failure to look for a connection between these sites is an oversight.*

We thank Rev#3 for the insightful suggestion to explore potential interactions between the two binding sites. We acknowledge that molecular dynamics (MD) simulations, such as those performed by Gumbart et al. and Hadden et al., could indeed provide valuable insights into the structural dynamics and potential cooperativity between these sites. Indeed, molecular dynamics of the HBV capsid by Perilla and Hadden has demonstrated significant flexibility in the capsid spikes and their interactions with neighboring subunits suggesting that the dynamics of binding sites could influence ligand accessibility and potential crosstalk.

We believe that our own previous structural studies together with data in this work provide substantial experimental evidence on this topic. In Makbul et al. 2021a (doi.org/10.3390/microorganisms9050956) we observed that peptide binding (particularly P2) did not stabilize the spikes; instead, the upper part of the spikes exhibited considerable wobbling. This variability mirrored the conformational diversity reported in MD simulations. Using local classification, we noted that the variability in the spike's upper region was greater when P2 was bound than in its absence. Additionally, in Makbul et al. 2021b (doi.org/10.3390/v13112115), we showed that peptide binding had little effect on the hydrophobic pocket beneath the mobile spike region, located in the more rigid part of the capsid. While we observed F97 in the D-monomer adopting two alternate rotamer orientations upon P2 binding this was not exclusive to P2, as similar changes were noted in the L60V mutant even without bound peptide.

We have updated the manuscript to briefly discuss this crosstalk, that provides additional context to our findings. Interestingly, only TX100—but not geraniol—completely flipped F97 into an alternate orientation, forming a new π-π stacking interaction with the mobile region of the spike. This finding suggests that interactions within the hydrophobic pocket are transmitted based on ligand specific interactions to the tips of the spikes. Thus, supporting and refining the concept of a crosstalk between binding sites, primarily initiated from the hydrophobic pocket in a ligand specific fashion.

> *The logic for proposing a terpene ligand is strained. Comparisons are made to HBs and the HDV delta antigen. However, HBs is myristoylated not farnesylated and delta antigen binds HBs not HBc.*

We have revised the text to clarify the rationale for testing terpenes as ligands, focusing instead on the specific properties of the hydrophobic pocket targeted by geraniol.

> *The authors suggest larger terpenes as binding agents, but there does not appear to be room for a longer molecule in the binding site. The authors do not discuss whether a longer molecule could be modeled in the site based on their density.*

We appreciate this observation and agree that the potential for larger terpenes to bind this site is not obvious from the structural data presented in this work. We have now included a more detailed visualization (Fig2D) and discussion of the hydrophobic binding pocket, based on the density observed in the presented geraniol structure and the previous triton structure and discuss its implications of the binding of larger hydrophobic molecules into the site (Fig 2D).

> *The authors note that the structure could explain molecular details of this site, but these are not discussed. A more complete analysis of the geraniol protein is necessary, including an estimate of the resolution of that density.*

We agree that a more complete analysis of the hydrophobic binding site was warranted. We have now expanded the discussion of the structural details of this binding site based on the geraniol-bound structure, the density and occupancy accounted by this ligand. These

additional details (Fig 2C,D and Fig 5) should provide a clearer understanding of the binding interactions observed.

> *The dimeric geraniol is marginally better binding than the monomer, two-fold, but this could be due to doubling the number of geraniols per ligand or due to an undefined interaction of the extended molecule with the surface of the capsid. A geraniol linker should be tested.*

The modest improvement in binding may indeed only reflect the doubled number of geraniols rather than linker-mediated avidity effects. Interaction of the linker with the capsid surface is ruled-out by the scrambled control that included the same linkers but did not show any capacity to bind.

> *Is the enhanced binding of dimer due to bivalent binding of dimer to one capsid? Is it a chance interaction of the linker with the surface of HBc, which is easily tested? Is it an avidity effect due to aggregation of capsids?*

Thank you for this insightful question. Our data suggest that the enhanced binding is due to bivalent interactions. To address the possibility of non-specific interactions from either the handle or the linker, we included a scrambled dimeric peptide as a negative control, which showed no binding. This rules out non-specific interactions from the linker or handle. Given this, we believe an additional monovalent control is unnecessary, as the scrambled control confirms that the binding is driven by the geraniol and peptide warheads alone. We have clarified this in the revised manuscript and appreciate your suggestion to strengthen the study.

> *The experimental analysis of point mutation of P1 is not analyzed beyond stating that it shows the importance of the core peptide sequence. Is there rationale for the effect of R3 to E and K10 to E mutation?*

We appreciate the reviewer's curiosity and request for a more detailed discussion of the P1 deep mutational scan data and its implications. The observed low mutation tolerance of the core peptide sequence SLLGRM regarding HBc binding is highly consistent with our prior structural data and binding studies in solutions (https://doi.org/10.3390/microorganisms9050956) as well as the results from the original phage library screening (M. R. Dyson, K. Murray, Proceedings of the National Academy of Sciences 1995, 92, 2194–2198), and the binding data presented here. Notably, the data set does not suggest that additional binding interfaces contribute to the aggregation seen with N-terminal elongated P1 and P2 versus the non-aggregating shorter SLLGRM. While the positional scan largely aligns with previous phage binding hierarchy and quantified ligands, we were previously prompted by surprising affinity gains for positive to negative amino exchanges in related peptides in same way as Rev#3: Specifically, “SLLGEM” has been predicted previously and here to show enhanced affinity over “SLLGRM”. Quantification in solution, however, could not confirm this enhanced HBV binding affinity (Makbul et al. 2021 Microorganisms), which could not be recapitulated by in solution quantification. In the revised version of the manuscript we now highlight the possible limited predictive power of this assay for positions where positively charged residues are exchanged by negatively charged residues (Figure legend of Fig 3D).

> *The fluctuations in Figure 3B could be largely magnification of noise due to changing the y-axis. The fluctuations can be characterized as standard variation, excluding the injections, to allow a quantitative judgment.*

Isothermal titration calorimetry heat fluctuations without injections are now shown in the supplementary information scaled to the same y-axis (Supplementary Figure 3D).

> *Molecular graphics throughout are too small and poorly labeled.*

We have revised the molecular graphics throughout the manuscript to increase their size and improve labeling for clarity. All figures are now provided in 500dpi.

> *In Figure 2, compounds 1 and 2 are pyrophosphates. The label in the figure should be corrected.*

Thank you for pointing this out. These compounds were removed for clarity.

> *In the introduction, the phrase "discontinuation frequently leads to relapse" should be changed to something less ambiguous.*

Thank you for highlighting this point regarding the phrasing in the introduction. We have revised the statement to more accurately reflect the clinical situation by specifying that stopping treatment often results in viral rebound and disease recurrence in many patients. This adjustment clarifies the intended meaning and addresses the ambiguity you identified. We hope this revision better aligns with the clinical context of HBV management and improves the overall clarity of the manuscript.

> *Define "functional cure" in the introduction.*

Thank you for your suggestion to clarify the term 'functional cure.' We have revised the manuscript and instead of ”functional cure” we mention the goal of sustained viral suppression without detectable HBV DNA and loss of hepatitis B surface antigen (HBsAg) without the need for continuous therapy. This should provide greater clarity for readers and improve the overall comprehensibility of the introduction.

> *The sentence beginning line 92 is not clear unless one has already read the paper. Figure 1 is not well described.*

Thank you for your valuable feedback regarding the clarity of this sentence and the legend of Figure 1. We have revised the text and legend to provide more context and improve the flow for readers who are unfamiliar with the specifics of the study. The revised version now clearly explains the targeted binding sites and the purpose of the bivalent binders at the beginning of the results section.

> *In line 235 the meaning is not clear. What is in excess? Is there free CPP in solution? Is it the charge on the CPP?*

We have clarified the passage as requested.

> *When describing peptide-induced aggregation, Figures 5 and 6, figure 1B is never referred to. Figure 1B would work better as part of Figure 6.*

We understand the reviewer’s suggestion. However, we decided to highlight and summarize the major findings and the underlying hypothesis early in the manuscript. We included Figure 1B at the beginning to allow readers to quickly grasp a core concept and outcome of our study.

We now however refer to Figure 1B and together with all the other changes hope that we have improved the clarity and quality of the manuscript.

We appreciate your constructive feedback and the opportunity to further refine the work.

https://doi.org/10.7554/eLife.98827.2.sa0